Antagonistic Effects of Point Mutations on Charge Recombination and a New View of Primary Charge Separation in Photosynthetic Proteins

K. Dubas,[1, 3] , S. Szewczyk,[1] Rafał Białek [1], G. Burdziński,[1] M. R. Jones,[2] K. Gibasiewicz[1]*

[1] Faculty of Physics, Adam Mickiewicz University, ul. Uniwersytetu Poznanskiego 2, 61-614 Poznań, Poland.

[2] School of Biochemistry, Medical Sciences Building, University of Bristol, University Walk, Bristol, BS8 1TD, UK

[3] Department of Optometry, Poznan University of Medical Sciences, ul. Rokietnicka 5d, 60-806 Poznań, Poland

* Corresponding author; e-mail: krzyszgi@amu.edu.pl; tel: +48 61 8296390

Abstract

Light-induced electron transfer reactions were investigated in wild type and three mutant *Rhodobacter sphaeroides* reaction centers with the secondary electron acceptor (ubiquinone Q_A) either removed or permanently reduced. Under such conditions, charge separation between the primary electron donor (bacteriochlorophyll dimer, P) and the electron acceptor (bacteriopheophytin, H_A) is followed by $P^+H_A^- \rightarrow PH_A$ charge recombination. Two reaction centers were used that had different single amino acid mutations that brought about either a three-fold acceleration in charge recombination compared to that in the wild type protein, or a three-fold deceleration. In a third mutant in which the two single amino acid mutations were combined, charge recombination was similar to that in the wild type. In all cases, data from transient absorption measurements were analyzed using similar models. The modeling included energetic relaxation of the charge separated states caused by protein dynamics and evidenced the appearance of an intermediate charge separated state, $P^+B_A^-$, with B_A being the bacteriochlorophyll located between P and H_A. In all cases, mixing of the states $P^+B_A^-$ and $P^+H_A^-$ was observed and explained in terms of electron delocalization over B_A and H_A. This delocalization, together with picosecond protein relaxation, underlie a new view of primary charge separation in photosynthesis.

Introduction

Studies of light-induced electron transfer (ET) reactions in photosynthetic proteins are important because similar electron transfer processes occur commonly in many other proteins and play vital functional roles. Moreover, the transformation of an excited electronic state into a charge separated state is a crucial reaction in many artificial photovoltaic devices, and so understanding this natural process may bring important guidelines on how to construct such devices for efficient energy conversion.

Photosynthetic reaction centers (RCs) are the pigment-protein complexes in which the energy of absorbed light is transformed into that of charge separated states.[1-4] The primary charge separation in RCs, the initial step of ET, occurs between a (bacterio)chlorophyll ((B)Chl) species, denoted P, and a nearby (bacterio)chlorin acceptor within a few picoseconds.[5-7]

One of the most widely studied RCs is that from the purple bacterium *Rhodobacter (Rba.) sphaeroides* (Figure 1A&B).[6-9] Three redox centres embedded in the protein are involved in the primary charge separation reaction, namely the dimeric BChl primary electron donor (P), a monomeric BChl, B_A, and a bacteriopheophytin (BPhe), H_A. The first relatively easily detectable charge-separated state, $P^+H_A^-$, includes only two of these centres.[5] However, more detailed studies have shown that the B_A BChl, located between P and H_A, is involved in the formation of the primary charge separated state either as a virtual electron carrier connecting P* to H_A in the superexchange mechanism[10] or, more likely, as a real intermediate electron carrier, according to the following sequential biphasic reaction:[11-12]

$$P^* \xrightarrow{\sim 3\ ps} P^+B_A^- \xrightarrow{\sim 1\ ps} P^+H_A^-. \quad (1)$$

The possibility that both of these sequential reactions are reversible has been indicated from detailed global and target analyses of transient absorption data.[13,14]

Following the formation of the state $P^+H_A^-$, the next forward ET step, completed within ~200 ps, takes place from H_A^- to the ubiquinone Q_A.[15-17] This forward reaction competes with back ET to P^+,[18] and this charge recombination reaction may be written in a simplified way as:

$$P^+H_A^- \rightarrow PH_A. \quad (2)$$

Since this charge recombination reaction occurs on a ~10-ns time scale,[19-25] it is rather difficult to observe in an "open" RC, *i.e.,* a RC in which forward ET to Q_A is possible and dominates because it is two orders of magnitude faster than recombination. A way to have access to this charge recombination reaction is to block the forward ET, either by removal of Q_A chemically[20,25] or genetically[27-28] or by its permanent reduction to Q_A^-.[20-22,26] The latter method

introduces an electric field inside the protein which affects both the primary charge separation[26,29-30] and the charge recombination.[31]

Similar to primary charge separation, studies of $P^+H_A^- \rightarrow PH_A$ charge recombination have demonstrated that it involves an intermediate state, $P^+B_A^-$.[26,32] Engagement of $P^+B_A^-$, together with dynamic relaxation of the protein triggered by the appearance of the charge separated states leading to a dynamic increase of the free energy gap between the states $P^+H_A^-$ and $P^+B_A^-$, was found to be responsible for multiexponential charge recombination.[33-35] Similar models have been used to explain variations in the charge recombination dynamics in a range of RCs with mutations[33,35] and over a range of temperatures.[34]

The dynamics of proteins span many orders of magnitude from picoseconds to seconds and beyond.[36] Their influence on ET in the RC has been postulated many times,[37-41] but their experimental dissection from the complex ET kinetics is a real challenge that is not often undertaken.[42-44] Perhaps the most impressive attempt was a demonstration that in a range of mutated RCs with manipulated interactions between P and B_A on the one hand, and the protein environment on the other hand, and thus with diverse P* decay kinetics (due to the primary charge separation), the kinetics of the protein, as monitored by the transient absorption signal from tryptophan residues at ~280 nm, was mutation-independent.[42] This apparent discrepancy was reconciled in the frame of a reaction-diffusion model, indicating that the protein dynamics actively trigger the primary charge separation rather than passively react to it. The detected kinetics of the protein occurred with 3-ps, 10-ps and 190-ps lifetimes. A protein dynamic occurring on 100-ps time scale was also proposed to prevent $P^+H_A^- \rightarrow PH_A$ charge recombination in open RCs.[35] Furthermore, the protein dynamics were hypothesized to affect the electron transfer from H_A^- to Q_A.[44] These experimental investigations were supported by theoretical approaches that considered protein dynamics in RCs on a time scale of up to 500-ps.[45-47]

In this contribution, we extend our previous kinetic model of primary charge separation and charge recombination in closed RCs, *i.e.*, in RCs with blocked ET from H_A^- to Q_A,[32,48] based on high quality transient absorption data and their detailed global and target analysis. The data were collected for wild type (WT) and three mutant RCs with blocked ET to Q_A. Two of these RCs, ELL and AMW, have been reported previously in the literature (see Materials and Methods for details). The ELL RC is characterized by a ~three-fold acceleration in charge recombination compared to the WT RC. Contrastingly the AMW RC, which is devoid of the Q_A ubiquinone secondary electron acceptor, shows a ~three-fold slower charge recombination compared to the WT RC. The opposing effects of these mutations on the kinetics of charge

recombination have been explained by their opposing influences on the free energy gap between the states $P^+H_A^-$ and $P^+B_A^-$ (Figure 1C) and thus, different degrees of access to the fast, activated charge recombination pathway (Figure 1A).[33] A third RC with both these mutations, denoted ELL/AMW, was newly constructed in this work in order to test the hypothesis that the opposing effects of the single mutations will cancel each other despite the different nature of the block of forward ET from H_A (i.e. Q_A reduction vs. its absence). Additionally, our thorough kinetic analysis resulted in a new perspective on the primary charge separation reaction (Eq. 1), which appears to be coupled with a fast protein relaxation on the time scale of a few picoseconds. On the other hand, a slower protein relaxation phase occurring on the ~500 ps to 2 ns time scale is responsible for the observed fast phase of the charge recombination. Thus, the protein dynamics appear to control ET reactions in RCs occurring on very different time scales ranging at least from picoseconds to nanoseconds.

Materials and Methods

Biological material

Purified RCs were prepared according to procedures described earlier.[33,49-51] In addition to WT RCs, the following mutant complexes were studied: ELL (Glu L104 replaced by Leu), AMW (Ala M260 replaced by Trp) and ELL/AMW (a combination of both single mutations; see Figure 1A for the location of the replaced amino acids). Mutation AMW results in the exclusion of the Q_A ubiquinone from its binding site.[27-28,43] Mutation ELL removes a hydrogen bond interaction with the H_A BPhe,[52] thus raising the free energy level of the state $P^+H_A^-$.[33,53] The double mutation is expected to combine these two effects.

For the transient absorption experiments, purified RCs were diluted in 15 mM Tris buffer (pH 8.0), containing 0.025% LDAO (N, N–dimethyldodecylamine-N-oxide). The final optical densities ($OD_{803nm,1cm}$) of the samples were 0.3-0.4. During the experiment, the RC solution was housed in a stirred quartz cell (2 mm path length). In order to close RCs, normal electron transfer from H_A^- to Q_A was blocked either by the absence of Q_A (caused by the AMW mutation) or by prereduction of Q_A to Q_A^- (in the WT and ELL RCs). To achieve Q_A reduction the samples were illuminated with a continuous background white halogen light (~1 mW/cm^2) in the presence of 10 mM of the external electron donor sodium ascorbate. Under this condition, low intensity background illumination creates the state $P^+Q_A^-$ and ascorbate re-reduces P^+ to P (Gibasiewicz et al. 2009),[32] resulting in the state PQ_A^-.

Transient absorption measurements and data analysis

Femtosecond UV-vis-NIR transient absorption spectra were collected using a Helios transient absorption setup (Ultrafast Systems).[54] The excitation beam was generated by a short-pulse titanium-sapphire oscillator (Mai-Tai, Spectra Physics, 70 fs) followed by a high-energy titanium-sapphire regenerative amplifier (Spitfire Ace, Spectra Physics, 100 fs, 1 kHz). The train of pulses exciting the sample was reduced to a 0.5 kHz repetition rate using a chopper. The 803 nm beam was split to form two beams: (1) pump (λ_{exc} = 803 nm) and (2) white light continuum probe pulses generated in a sapphire plate (440 – 780 nm).[54] The remaining 803 nm photons in the probe pulse were filtered out by a BG 38 cut-off filter before the sample to avoid additional excitation of the sample. The instrument response function was approximately 200 fs wide. The pump pulse energy was approximately 1 μJ at the sample position and this relatively high intensity did not introduce any unwanted nonlinear effects. All experiments were performed at room temperature. The data were acquired in a ~3-ns time window. For each delay time t, the ΔA(t) was calculated from recorded 1000 probe spectra (500 spectra with the pump, and 500 spectra without the pump). The whole kinetics were collected twice, once with gradually increasing delay times between pump and probe and after that with gradually decreasing times, in order to ensure there were no systematic changes in the samples during the experiments. The 3-ns width of the experimental time window was smaller than the values of the slowest lifetimes obtained from fitting the experimental results. For this reason the nanosecond components reported below should be treated with caution as very approximate estimates of the slow charge recombination kinetics.

The results were corrected for spectral chirp of the white-light continuum using SurfaceXplorer software (Ultrafast Systems). Glotaran software was used to perform global and target analyses.[55] Steady-state absorption spectra were collected using a Hitachi-1900 UV/VIS spectrophotometer.

Results and Discussion

Global analysis

Femtosecond time-resolved absorption changes between 470-720 nm, triggered by the 803-nm ~100-fs excitation flashes, were recorded over a ~3-ns time window for the WT RC and the three mutant complexes. Figure 2 presents decay associated difference spectra (DADS) from a global analysis of these data. An appearance of photobleaching (PB) and excited state absorption (ESA) is presented as positive and negative DADS, respectively, whereas the

polarities of DADS depicting decay of PB and ESA are inverse. The two fastest subpicosecond components (of ~150 and ~300 fs lifetimes), depicting energy transfer from initially excited B* to P,[56-60] with a possible minor contribution of direct charge separation from the state B*,[61-62] were obtained for all of the RCs but are not of the primary interest in this paper and therefore are neither shown nor discussed in detail. All four datasets were characterized by four remaining components with lifetimes ranging from ~2 ps to ~10 ns (Figure 2). The corresponding DADS in each of these datasets were of roughly similar lifetime, shape and origin, but had different relative contributions.

The similarity in lineshape of corresponding DADS for the four RCs is demonstrated in Figure 3. The main features of the DADS of the component with a 2.2-2.9-ps lifetime (Figure 3A) was a positive band at ~595 nm and a broad negative band with a relatively flat minimum between 650 and 690 nm. Both these features are clearly ascribable to the formation of the B_A^- anion due to ET from P* to B_A: the band at ~595 nm is due to the appearance of photobleaching of the B_A Q_x transition band, whereas the trough at 650-690 nm is due to the appearance of transient absorption of B_A^-.[63] The features around ~540 nm may be due to a mixture of an electrochromic shift of H_A upon the formation of B_A^- and formation of a certain amount of H_A^- simultaneous with the formation of B_A^-.

The DADS of the component with a 5.5-7.5 ps lifetime (Figure 3B) were also dominated by two features which this time were ascribable to the formation of the H_A^- anion. These were a positive band peaking, depending on the sample, between 535 and 541 nm, and a negative band at ~665 nm (WT and AMW) or at ~631 nm (ELL and ELL/AMW). The origin of these two features is analogous to that of the corresponding features described above for B_A^- formation: the positive band is due to the appearance of photobleaching of the H_A Q_x band, and the negative one to the appearance of the absorption of H_A^-.[63] Interestingly, the position of the negative band was strongly blue-shifted from 665 nm in the WT and AMW RCs to 631 nm in the ELL and ELL/AMW RCs. This effect, together with a smaller diversity in the 535-541 nm band position, is a result of breaking of a hydrogen bond between glutamate 104 of the L subunit and the H_A BPhe in the ELL and ELL/AMW mutants, and was reported earlier.[48] It is worth noting that the sharp shapes of the transient absorption bands of H_A^- at 665/631 nm are clearly different from the analogous flat broad bands of B_A^- at 650-690 nm (Figure 3A). The two main features at 535-541 and 665/631 nm are accompanied by smaller and more difficult to explain changes in the ~600 nm region. In the spectra of the WT, AMW and ELL/AMW RCs there is a negative band in this region. This could be due to decay of B_A^- photobleaching caused by electron transfer from B_A^- to H_A. Conversely, in spectra of the ELL RC, the band at ~600 nm is

positive. This indicates that, on the 5.7-ps time scale, some formation of B_A^- still occurs in the ELL RCs in parallel with the formation of H_A^-. Apparently, the 5.5-7.5 ps DADS, similarly to the 2.2-2.9-ps DADS, depict a mixed contribution from at least two processes. A non-trivial novelty of the presented global analysis was the clear resolution of the ~2.5-ps and ~6-ps processes, which previously were lumped together within a single kinetic process.[32,48]

It is also notable to compare the relative contributions of the 2.2-2.9-ps DADS (Figure 2, black spectra) and the 5.5-7.5 ps DADS in different samples (Figure 2, red spectra). The extreme cases are AMW, for which the B_A^- photobleaching formation band at ~600 nm is the smallest, and ELL, for which the B_A^- photobleaching formation band is the largest.

The third common component had a lifetime of hundreds of picoseconds (Figure 3C), ranging from 490 to 590 ps for the WT, ELL and ELL/AMW RCs. (For WT and ELL RCs similar kinetic components were resolved previously in transient absorption experiments performed and analyzed over a 100-ns experimental time window.[33]) For these three RCs the main features of this third component were a negative band at 598 nm and a broad flat positive band between 620 and 700 nm. These features resemble inverted spectra from Figure 3A assigned to the formation of B_A^-, and thus are assigned partly to the decay of B_A^- caused by $P^+B_A^- \rightarrow PB_A$ recombination. Due to this assignment, a part of the 598-nm band has to be ascribed to the decay of P^+ photobleaching. Importantly, the 490-590-ps DADS were additionally contributed to by negative bands peaking at 539 nm (ELL, ELL/AMW) or 546 nm (WT). These bands reveal simultaneous decay of a fraction of H_A^- caused by an equilibrium established between the two states: $P^+H_A^- \leftrightarrow P^+B_A^-$. Since the 539-546-nm signal from H_A^- is ~3 times smaller than the ~598-nm signal from B_A^-/P^+, we estimate that the states $P^+H_A^-$ and $P^+B_A^-$ are roughly isoenergetic on the time scale of a few hundreds of picoseconds. This estimation originates from a rough assumption that the differential extinction coefficient for H_A^-/H_A at ~540 nm is the same as those for B_A^-/B_A and P^+/P at ~600 nm (see also DADS in Figure 3D).[63] Under such an assumption, one-third of the ~600-nm band is due to the decay of B_A^- photobleaching, one third is due to P^+ from the state $P^+B_A^-$, and one third is due to P^+ from the state $P^+H_A^-$. Thus, similar total contributions of $P^+B_A^-$ and $P^+H_A^-$ photobleaching (at ~540 nm and ~600 nm) reveal the isoenergetic character of these two states: the same amount of the oscillator strength from $P^+B_A^-$ and $P^+H_A^-$ is lost within ~500 ps. This issue is further commented below when discussing the shape of the "$P^+B_A^-$" SADS.

The third component for the AMW RC had a shorter 160-ps lifetime, with a partially differently shaped DADS compared to the equivalent 490-590-ps DADS for the other RCs (Figure 3C). A negative band at ~600 nm is accompanied by a positive band at 543 nm of

similar amplitude. This indicates that the process underlying the 160-ps DADS was a slow electron transfer from B_A^- to H_A. This assignment is further confirmed by the shape of this DADS between 620 and 720 nm, which looks like a wide positive band (due to decay of transient absorption of B_A^-) interrupted by a sharper negative band at ~670 nm (due to the formation of transient absorption of H_A^-). The shape of this DADS resembles that of the 5.5-ps DADS, except for a higher contribution of the B_A^- decay features in the case of the former (see Figure S1). However, considering that the 160-ps DADs is very small, this difference may be due to some inaccuracy of the measurement (compare the respective DADS in Figure 2B).

The DADS of the fourth, slowest component with a 4.1-10-ns lifetime showed features easily ascribable to $P^+H_A^-\rightarrow PH_A$ recombination (Figure 3D). The shapes of these DADS were particularly similar to one other for the WT and AMW RCs. For these the negative signal at 598 nm is due to P ground state absorption recovery (decay of Q_x band photobleaching caused by transient formation of P^+ cation), whereas the negative band at 544 nm is due to a similar recovery of the H_A Q_x band. These features are complemented by positive bands at ~665 nm showing the decay of transient absorption of H_A^- anion (compare this band to the respective negative bands in Figure 3B depicting the formation of H_A^-). The equivalent DADS for the ELL and ELL/AMW RCs had differences that were attributable to the ELL mutation. In a similar fashion to the 5.5-7.5-ps DADS assigned mostly to the formation of the state $P^+H_A^-$, both the photobleaching band at ~535 nm and transient absorption bands at 634 nm were blue-shifted compared to the bands at ~545 nm and 665 nm, respectively, in the WT and AMW RCs. Generally, the shapes of the 4.5-4.8-ns DADS for the ELL and ELL/AMW RCs are very similar to each other except for somewhat larger H_A photobleaching band at ~535 nm for the ELL/AMW RC.

The amplitudes of the 490-590-ps DADS, relative to those of the slowest 4.1-4.8-ns DADS, were very much different in the three RCs (Figure 2). For the ELL RC the amplitude of the 490-ps DADS was, at all wavelengths, a few times larger than that of the 4.5-ns DADS, whereas in the WT and ELL/AMW RCs an opposite effect was observed, with the amplitudes of the 4.1/4.8-ns DADS being a few times larger than those of the 490/510-ps DADS. Thus overall $P^+H_A^-\rightarrow PH_A$ recombination in the ELL RC was dominated by the ~0.5-ns component, whereas in the WT and ELL/AMW RCs the 4.1/4.8-ns recombination dominated. On the other hand, in the AMW RC, the $P^+H_A^-\rightarrow PH_A$ recombination occured exclusively within ~10 ns lifetime.

A comparison of the kinetics at three selected wavelengths, demonstrating these differences in the $P^+H_A^-\rightarrow PH_A$ recombination dynamics, is presented in Figure 4. The

accelerated kinetics in the the ELL RC, and decelerated kinetics in the AMW RC, relative to the WT, are in line with earlier reports.[33,48] In the newly constructed double mutant, ELL/AMW, the opposing effects of the two mutations largely cancelled one another. This is particularly evident at the 565 and 665/635 nm wavelengths where the charge recombination kinetics for the ELL/AMW and WT RCs are almost identical (Figure 4 A&C).

Finally, it should be noted that in order to obtain a fully satisfactory fit for the ELL RC, an additional kinetic component of 75 ps had to be added (Figure 2C). Its amplitude was very small and the shape of its DADS resembled the shape of the 160-ps DADS for the AMW RC (compare Figs. S1 and S2). This indicates again a small fraction of slow electron transfer from B_A^- to H_A^-. It is difficult to judge if the minor 75/160-ps processes are natural or artificially induced by isolation/storage procedures.

Target analysis – species associated difference spectra

The results of global analysis (Figure 2) indicated, in all the samples, a biphasic charge separation with lifetimes of ~2.5 and ~6 ps associated mostly with the formation of $P^+B_A^-$ and $P^+H_A^-$ states, respectively. This encouraged us to propose a physical model with a separate compartment depicting a pure $P^+B_A^-$ state. A compartmental model consistent with the global analysis and yielding interpretable spectra, applied to all four RCs, is shown in Figure 5. Two compartments depicting the excited state of B, B_1* (80% of initial population) and B_2* (20% of initial population), were necessary to reconstruct the two subpicosecond phases resolved in the global analysis. Four more compartments were introduced: P* (excited state of the primary donor), "$P^+B_A^-$" (a dominant $P^+B_A^-$ state), and two sequentially formed $P^+H_A^-$ states: "$(P^+H_A^-)_1$" and $(P^+H_A^-)_2$. Different forms of the $P^+H_A^-$ state relating to different relaxation states of the protein environment have been proposed previously.[13-14,21-22,31,43,64-65]

The results of the target analysis is presented in a form of species associated difference spectra (SADS, Figure 6). Unlike DADS which are the spectra of individual kinetic components, SADS are the difference spectra of individual transient species relative to the ground state absorption spectrum of the samples: thus photobleaching of the ground state absorption is represented by negative bands, whereas transient absorption is represented by positive bands. Overall, the shapes of respective SADS for all four RCs were rather similar to one another (Figure 6). The shape of the P* spectrum was almost identical for the four RCs and showed photobleaching exclusively at 600 nm, as expected (Figure 6A). Additionally, one can see a very strong excited state absorption "baseline" that was tilted up towards longer wavelengths and covered the whole spectral region investigated.

The "$P^+B_A^-$" SADS were also similar for all the RCs, and particularly so within the pairs WT&AMW RC and ELL&ELL/AMW RC (Figure 6B). Interestingly, however, they show photobleaching not only at ~600 nm, as was initially expected for the pure $P^+B_A^-$ state, but additionally an H_A photobleaching band at 535 nm (ELL&ELL/AMW RC) or at 544 nm (WT&AMW RC). It was notable that the shapes of these SADS for the WT, ELL and ELL/AMW RCs resembled the shapes of the 490/590 ps DADS (Figure 3C). Moreover, for the AMW RC, the SADS was similar to that resolved for the WT RC, thus making us confident that the proposed compartmental model is proper. Similarly, as was noted above when describing the 490/590 ps DADS, the photobleaching signal at ~600 nm was about three times larger than the photobleaching signal at 535/544 nm. This observation, together with the assumption that the differential extinction coefficient for H_A^-/H_A at ~540 nm is the same as those for B_A^-/B_A and P^+/P at ~600 nm, indicates that the "$P^+B_A^-$" SADS is equally contributed to by the states $P^+B_A^-$ and $P^+H_A^-$ in all the samples under study (see above). This equal contribution again indicates the isoenergetic character of these two states. In such a case, the latter state could be consequently labeled $(P^+H_A^-)_0$ in order to distinguish it from the states "$(P^+H_A^-)_1$" and $(P^+H_A^-)_2$ resolved in our model (Figure 5). Thus, the compartment "$P^+B_A^-$" would be an equilibrated state $P^+B_A^- \leftrightarrow (P^+H_A^-)_0$. Since we were not able to separately resolve the states $P^+B_A^-$ and $(P^+H_A^-)_0$ we think that such an equilibrium is realized by very fast forward and backward electron transfer between B_A and H_A. In the case of extremely fast electron transfer between these two species, the electron may be regarded as delocalized over B_A and H_A. In such a case, the state "$P^+B_A^-$" should be better labeled as $P^+(B_AH_A)_0^-$. An alternative explanation for the mixed character of the state "$P^+B_A^-$" could be faster formation of the state $P^+H_A^-$ in a fraction of RCs showing an alternative, faster, charge separation pathway: $B^* \rightarrow B^+H_A^- \rightarrow P^+H_A^-$.[61-62] However, since this pathway was observed only for open WT RCs at 77 K and in a specific mutant, we regard this explanation as less likely. Additionally, the (quasi)isoenergetic equilibrium $P^+B_A^- \leftrightarrow P^+H_A^-$ lives for up to ~500-ps (Figure 3C) that would be difficult to reconcile with the heterogeneous origin of the state "$P^+B_A^-$".

The third SADS labeled "$(P^+H_A^-)_1$" most likely also does not represent a pure state for any of the RCs. This can be judged from comparison of the shapes of these SADS (Figure 6C) with those of "$P^+B_A^-$" (Figure 6B) and $(P^+H^-)_2$ (Figure 6D) for the respective RC. The amount of H_A^- contribution revealed by the amplitude of the 540-nm band relative to that of the ~600-nm band systematically increased from Figure 6B through C to panel D for each of the samples. The $(P^+H^-)_2$ SADS is believed to be a relatively pure relaxed form of $P^+H_A^-$ (Figure 6D). For the WT and AMW samples, the $(P^+H_A^-)_2$ SADS were highly similar to one another and both

showed a photobleaching at ~540 nm (assigned to H_A^-) that was slightly deeper than that at ~600 nm (assigned to P^+; Figure 6D). In the previous reports, similar spectral features were interpreted as indicating a pure relaxed state $P^+H_A^-$.[32,48] Although the $(P^+H^-)_2$ SADS of the ELL RC is somewhat different due to the specific mutation affecting H_A, the relationship between the minima of the ~540-nm and ~600-nm bands was similar to those in the WT and AMW RCs (Figure 6D). The $(P^+H^-)_2$ SADS for the ELL/AMW RC is characterized by somewhat deeper band at ~540 nm but this may be a synergistic effect of the double mutation.

Returning to the "$(P^+H_A^-)_1$" SADS (Figure 6C), its shape was intermediate between those of the "$P^+B_A^-$" and $(P^+H_A^-)_2$ SADS (Figure 6B&D). This is most obvious for the ELL RC (compare the amplitudes of the three spectra at ~540 nm or at ~635 nm in Figure 5C) but was also seen for the remaining RCs. These intermediate shapes of the "$(P^+H_A^-)_1$" spectra indicate admixture of the state $P^+B_A^-$ in the "$(P^+H_A^-)_1$" compartment.

Regarding the mixed character of the states "$P^+B_A^-$" and "$(P^+H_A^-)_1$" it should be noted that a similar mixing was proposed previously for open *Rb. sphaeroides* RCs by Zhu et al.[66] and explained in the context of adiabatic ET from P* to (B_AH_A). We cannot completely rule out the possibility that even more complex modeling, including RC heterogeneity, could result in the resolution of exclusively pure $P^+B_A^-$ and $P^+H_A^-$ states as was obtained in an alternative modeling of the simpler system of open RCs with neglected charge recombination.[66] However, closed RCs, particularly those clearly showing $P^+B_A^- \rightarrow PB_A$ charge recombination on a time scale of hundreds of picoseconds, may favour delocalization of electron between B_A^- and H_A^- much more than open RCs do.

Target analysis – intrinsic lifetimes

Because the common compartmental model generally yielded similar shapes of the respective SADS for the different RCs (Figure 6), significant differences in their kinetics (Figure 4) have to be accounted for by the differences in the intrinsic rate constants or their reciprocals, intrinsic lifetimes, connecting the individual compartments (see the compartmental models in Figure 5). The subpicosecond lifetimes of ~100-300 fs (τ_1 and τ_6) accounted for B*→P* energy transfer in all the samples. The lifetime of the P*→"$P^+B_A^-$" charge separation (τ_2) ranged from ~2 to ~3 ps. The next forward reaction, "P^+B_A"→"$(P^+H_A^-)_1$" was accompanied by a back reaction in all the RCs except AMW (Figure 5B). The lack of this back reaction in the AMW RC may be explained by the lack of the electrostatic repulsion between the missing Q_A^- and H_A^- (such repulsion is present ELL and WT RCs). The lifetime of the "$P^+B_A^-$"→"$(P^+H_A^-)_1$" reaction (τ_3) in the WT and AMW RC was 5.5-5.7 ps and the lifetime of the back reaction

in the WT RC was 360 ps (τ_8). The ratio of these lifetimes for the WT RC yields a significant free energy gap, ΔG, of 104 mV between these states (Table 1) estimated from the formula:

$$\Delta G = kT \ln(\tau_8/\tau_3) \quad (3)$$

This gap results in a population of only 1.6% of the more energetic state "$P^+B_A^-$". Still, the back reaction is necessary, together with "$P^+B_A^-$"→PB_A charge recombination characterized by lifetime τ_7 = 200 ps, in order to justify the "leakage" of the "$P^+B_A^-$" state clearly demonstrated by the 490-ps DADS (Figs. 2A and 3C). This value of 200 ps was taken from the literature[32,67-68] and was fixed for all samples in our modelling. The value of 490 ps is limited by the 500-ps lifetime (τ_4) characterizing the next forward reaction, "$(P^+H_A^-)_1$"→$(P^+H_A^-)_2$. Overall, four intrinsic lifetimes (τ_3, τ_4 ,τ_7, τ_8), define together the efficiency of the "$P^+B_A^-$"→PB_A charge recombination and an apparent lifetime of the "$P^+B_A^-$" state (Figs. 5A and 3C). The second route of charge recombination, $(P^+H_A^-)_2$→PH_A, without the involvement of the state "$P^+B_A^-$", was characterized by the lifetime τ_5 = 4.1 ns (Figure 5A).

In the AMW RC, the free energy gap between the states "P^+B_A" and "$(P^+H_A^-)_1$" is expected to be significantly larger than that for the WT RC due to the lack of electrostatic repulsion between Q_A^- and H_A^- in the former sample. Because of this, and because of the very fast "P^+B_A"→"$(P^+H_A^-)_1$" reaction (5.5 ps), the "$P^+B_A^-$"→PB_A charge recombination characterized by a lifetime τ_7 of 200 ps could have been neglected in the model (Figure 5B) without impairment of the fit quality. The "$(P^+H_A^-)_1$"→$(P^+H_A^-)_2$ reaction with a 165-ps intrinsic lifetime is related with the small 160-ps DADS shown in Figure 2B and with a very small spectral evolution shown in Figure 5B. In the AMW RCs, the only effective route of charge recombination is $(P^+H^-)_2$→PH which takes 10 ns (Figure 5B). The lack of the fast recombination route via the state $P^+B_A^-$, together with the slowest direct $(P^+H_A^-)_2$→PH_A recombination, are the reasons why AMW is the mutant with the slowest charge recombination kinetics (Figure 4).

Conversely, charge recombination is the fastest in the ELL RC (Figure 4). This is reflected by the specific combination of τ_3, τ_4 and τ_8 lifetimes. Firstly, the ratio of forward and backward lifetimes, τ_8/τ_3 = 2.4, is much smaller than that for the WT (63; Table 1). Thus, the population of the state "$P^+B_A^-$", being in equilibrium with "$(P^+H_A^-)_1$", is much larger (29%) than in the WT RC (1.6%; Table 1). Moreover, the "$(P^+H_A^-)_1$"→$(P^+H_A^-)_2$ reaction lifetime (τ_4) is 2 ns, four times larger than that for the WT RC. These two factors ensure together that the equilibrated state "P^+B_A"↔"$(P^+H_A^-)_1$" decays very effectively via "$P^+B_A^-$"→PB_A charge recombination. Consequently, the competitive alternative charge recombination route, $(P^+H^-)_2$→PH, is much less effective, in line with much lower amplitudes of the 4.5-ns DADS compared to the 590-ps DADS (Figure 2C). As a result, the overall charge recombination

kinetics in the ELL RC is dominated by the 590-ps component (Figs. 2C and 4). At this point it should be noted that the common compartmental model applied to the ELL sample (Figure 5) results in six DADS (see Figure S3 and the corresponding chapter in SI) and not seven as described above in the *Global analysis* section. The 7-exponential global analysis model gave a somewhat better fit due to introducing the small 75-ps component (Figure 2C). However, we were not able to generate reliably a more complex compartmental model, with an additional compartment, reproducing the seven lifetimes obtained in the global analysis. Consequently, the relatively large value of τ_3 = 26 ps (Figure 5C) may be an overestimation resulting from the 6-compartmental model, whereas the 7-exponential global fit suggests a much faster second phase of charge separation, of the order of 6 ps (Figure 2C), similar to those for the remaining RCs (Figure 2).

For the ELL/AMW RC (Figure 5D), the value of τ_8/τ_3 is 7.3 which is three times larger than the 2.4 obtained for the ELL RC (Table 1), and therefore the "P^+B_A"↔"$(P^+H_A^-)_1$" equilibrium is shifted more towards "$(P^+H_A^-)_1$" in the double mutant. On the other hand, τ_4 = 640 ps which is three times less than the 2 ns seen for the ELL RC. Both these differences make the "fast route" of charge recombination, via the state "$P^+B_A^-$", less efficient in the ELL/AMW RC than in the ELL RC. Consequently, charge recombination for the ELL/AMW RC occurs mostly via the "slow route" (direct $(P^+H_A^-)_2 \rightarrow PH_A$ recombination; see also amplitudes of the 510-ps and 4.8-ns DADS in Figure 2D) and thus is slower than for the ELL RC (Figure 4). When comparing the lifetimes obtained for the ELL/AMW RC with those for the WT, one can see that the values of τ_8/τ_3 fraction (Table 1) and τ_4 promote a higher efficiency of charge recombination via the "slow route" in the WT RC ($(P^+H_A^-)_2 \rightarrow PH_A$). On the other hand, the direct $(P^+H_A^-)_2 \rightarrow PH_A$ charge recombination lifetime is somewhat slower for the ELL/AMW RC (τ_5 = 4.8 ns) than for the WT (4.1 ns). The net result of these differences is generally faster charge recombination dynamics in the ELL/AMW RC than in the WT (compare DADS in Figure 2A&D and kinetics in Figure 4B) but at some wavelengths, the kinetics for both samples are very similar to one another (Figure 4A&C). A clear effect of the double mutation compared to the AMW RC is an acceleration of the direct charge recombination, $(P^+H_A^-)_2 \rightarrow PH_A$ (τ_6), from 10 ns (characteristic of AMW) to 4.8 ns.

Energetic model

The opposing effects of the ELL and AMW mutations on the kinetics of $P^+H_A^- \rightarrow PH_A$ recombination largely cancel one another in the double mutant ELL/AMW. This observation supports the model in which the overall $P^+H_A^- \rightarrow PH_A$ recombination dynamics are controlled

by the free energy gap between the states $P^+H_A^-$ and $P^+B_A^-$, independent of the nature of modifications leading to the change in this free energy gap. In the AMW RC the free energy gap is increased relative to that in the WT RC (Figure 1A) by removing the repulsive electrostatic interaction between Q_A^- and H_A^- that is characteristic for a WT RC with a permanently reduced quinone, Q_A^-. This was achieved by removal of the quinone Q_A from its binding pocket through the AMW mutation. On the other hand, in the ELL RC, the free energy gap is decreased relative to that in the WT RC by removing the hydrogen bond between a glutamate side chain and H_A, which in the WT RC stabilizes the state $P^+H_A^-$.[33] Both mutations affect H_A on its distal side from P and B_A, and they should therefore not affect the properties of B_A and P (Figure 1A). Indeed, whereas the ELL mutation clearly shifts the H_A Q_x and anionic absorption bands (Figure 3B-D), no evident effect of this or the AMW mutation on the B_A or P bands was observed. Thus we propose that the cancellation of the opposing effects of the ELL and AMW mutations on the charge recombination kinetics in the double mutant originates from the cancellation of their influence on the free energy level of the state $P^+H_A^-$ relative to that of $P^+B_A^-$ (Figure 1C). However, it was shown previously that the state $P^+H_A^-$ evolves in time due to the relaxation of the protein environment leading to a gradual free energy gap increase between the states $P^+H_A^-$ and $P^+B_A^-$.[13-14,21-22,31,43,64-65] So the question arises of how to relate the temporal evolution of this gap with the influence of the mutations on it.

In our target analysis we were not able to resolve a pure $P^+B_A^-$ state. In all samples, the compartment "$P^+B_A^-$" contains a contribution from the state $P^+H_A^-$ (Figure 5) indicated by a negative band at ~540 nm due to H_A photobleaching. Similarly, the compartment "$(P^+H_A^-)_1$" describes not a pure $P^+H_A^-$ state but one which contains a contribution from $P^+B_A^-$, as noted above. Therefore, in our energetic model (Figure 7), consistent with the target analysis, we replaced the labels "$P^+B_A^-$" and "$(P^+H_A^-)_1$" with the labels $P^+(B_AH_A)_0^-$ and $P^+(B_AH_A)_1^-$, respectively. For consistency we also replaced the label $(P^+H_A^-)_2$ with $P^+(B_AH_A)_2^-$. These replacements (except for the last one) are not only formal ones but they bear interpretational consequences. In such an approach, each of the discrete states $P^+(B_AH_A)_i^-$ represents a charge separated state related to a different protein relaxation state. In each of these states, the electron is delocalized over B_A and H_A. However, the degree of this delocalization evolves in time after the excitation (Figure 7). In the state $P^+(B_AH_A)_0^-$, where the contributions of the states $P^+B_A^-$ and $P^+H_A^-$ were shown above to be roughly the same for all the RCs (Figure 6B), the delocalization ratio is ~50:50. This delocalization is shifted towards H_A^- in the state $P^+(B_AH_A)_1^-$, and the electron is assumed to be fully localized on H_A in the state $P^+(B_AH_A)_2^-$. In order to estimate the delocalization ratio between B_A and H_A in the state $P^+(B_AH_A)_1^-$, we compared the

amplitudes of the "$(P^+H_A^-)_1$" SADS at ~540 and ~600 nm with those of the corresponding $(P^+H_A^-)_2$ SADS (see Figure S4 and corresponding chapter in SI for details). As a result, the B_A/H_A delocalization ratio was estimated to be ~3:97 for the WT RC, 5:95 for the AMW RC, 30:70 for the ELL RC, and 14:86 for the the ELL/AMW RC (Table 1). In Figure 7, the electron localization on B_A vs H_A is proportional to the areas of circles representing the two molecules. We identify the electron delocalization ratios with the population ratios of the virtual pure states $P^+B_A^-$ and $P^+H_A^-$ within the state $P^+(B_AH_A)_1^-$, and thus the delocalization ratios allow estimation of the free energy gaps, ΔG_1 (Eq. S5), between these virtual states (Table 1). On the other hand, Figure 7 shows the free energy gaps between the states $P^+(B_AH_A)_0^-$ and $P^+(B_AH_A)_1^-$ obtained directly from the target analysis (Table 1, Eq. 3).

It is not clear whether the mixing between the states $P^+B_A^-$ and $P^+H_A^-$ within the states $P^+(B_AH_A)_0^-$ and $P^+(B_AH_A)_1^-$ is strictly quantum mechanical mixing or whether it comes from fast transitions between pure $P^+B_A^-$ and $P^+H_A^-$ states. We tend to think that initially, in the state $P^+(B_AH_A)_0^-$, the electron is delocalized quantum-mechanically between B_A^- and H_A^- in line with the suggestion by Zhu et al.[66] The state $P^+(B_AH_A)_1$ may depict the situation of fast transitions between pure $P^+B_A^-$ and $P^+H_A^-$ states.

The model shown in Figure 7 indicates that the initial state $P^+(B_AH_A)_0^-$, in which the virtual pure states $P^+B_A^-$ and $P^+H_A^-$ are isoenergetic, appears in all the RCs under study. Apparently, the mutations do not affect the initial energy level of $P^+H_A^-$ relative to that of $P^+B_A^-$. This may seem surprising. However, it should be noted that charge separation is not heavily affected by the mutations (Fig. 3A), and it may be that equal charge distribution between B_A^- and H_A^- is a requirement for the fast charge separation observed both in the WT RC and in the mutant complexes. Investigation by other techniques would be valuable to verify the isoenergetic character of initial $P^+B_A^-$ and $P^+H_A^-$ states. Measurements of delayed fluorescence could provide information on the free energies of all the states relative to P*. The energies might be rationalized by electrostatics calculations and molecular dynamics (MD) simulations. MD simulations also could help to elucidate the relaxations of the protein (see below).

Temporal evolution from the state $P^+(B_AH_A)_0^-$ to the state $P^+(B_AH_A)_1^-$ and then to $P^+(B_AH_A)_2^-$ is an individual feature of each of the RCs (Figure 7). The relaxation process is approximated by two exponential phases: a fast one of 5.5-26 ps lifetime and a slow one of 165-2000 ps lifetime. The fast phase of relaxation for the WT, AMW and ELL/AMW RCs, of 5.5-8.8 ps lifetime, occurs in parallel with (partial) localization of the electron on H_A, proposed to be a consequence of very rapid protein relaxation. Consequently, we think that this phase of a few-picoseconds, classically described as a second phase of charge separation, is in fact the

protein response to a single step charge separation reaction $P^* \rightarrow P^+(B_AH_A)_0^-$ occurring with a ~2-3-ps lifetime (Figs. 2&5). The model shows that this phase is slower for ELL (26 ps). This could be an effect of particularly effective electrostatic repulsion between Q_A^- and the electron to be transferred from P* to the pair B_AH_A in this mutant. However, it is also possible that the large value of 26 ps results from inaccuracy of the target model containing only six compartments, whereas in the seven-component global fit, the 5.7-ps phase could have been resolved similar to those in the remaining samples (Figure 2C).

Unlike the unrelaxed state $P^+(B_AH_A)_0^-$, the properties of the first relaxed state $P^+(B_AH_A)_1^-$ is clearly mutation-dependent. Its free energy level is clearly shifted up in the ELL RC and shifted down in the AMW RC, relative to its position in the WT RC (Figure 7). In the case of the ELL/AMW RC, this level is inbetween those of the ELL and AMW RCs in line with predictions summarized in Figure 1C. Estimation of the free energy gaps between the states $P^+(B_AH_A)_0^-$ and $P^+(B_AH_A)_1^-$, ΔG, was possible due to the back reactions modelled in the target analysis (Figs. 5 and 7). We postulate that this reversibility holds for protein relaxation states and not for the $B_A^- \leftrightarrow H_A^-$ equilibrated electron transfer. Different degrees of localization of the electron on H_A in these two states is only a consequence of two different protein relaxation or conformational states. The observed correlation between the ΔG gap and the degree of electron localization on H_A (the larger is ΔG the stronger is localization of the electron on H_A) is a secondary effect of the protein relaxation.

In our model, the states $P^+(B_AH_A)_0^-$ and $P^+(B_AH_A)_1^-$ show the possibility of charge recombination by back electron transfer from B_A^- to the ground orbital of P^+, and this reaction is particularly effective when the ΔG gap is small. Thus, the ΔG gap, together with the second relaxation step lifetime (165-2000 ps; Figure 7) controls the branching between the fast charge recombination route (via $P^+B_A^-$) and the slow one (direct $P^+H_A^- \rightarrow PH_A$ charge recombination). The ΔG gap is particularly large (and unmeasurable because of unresolved back reaction) in the AMW RC. Consequently, the only charge recombination in this sample is the direct one and thus is particularly slow.

In summary, we were able to resolve two phases of the protein relaxation – a faster one (5.5-26 ps) and a slower one (165-2000 ps). The second phase of relaxation leads to the state $P^+(B_AH_A)_2^-$ that was assumed to recombine only directly within ~4-5-ns (WT, ELL, ELL/AMW RCs) or ~10 ns (AMW RC). However, due to the time window of the transient absorption experiment being limited to ~3 ns, the values of lifetimes of 4-10 ns may be rather inaccurate. Indeed, in addition to subnanosecond components, two more recombination phases have been resolved, ranging from ~1 to ~20 ns, in experiments performed in wider time windows.[21-22,33,69]

Thus, it is very likely that the single ~4-10-ns phases reported in this paper are actually an approximation of two different phases occurring over nanosecond time-scale. It was proposed before that the relaxed $P^+H_A^-$ state decaying on a few-nanosecond time scale is kinetically faster than the next $P^+H_A^-$ state (decaying within >~10 ns) due to equilibrium with the state $P^+B_A^-$ persisting to the nanosecond time scale.[69]

Primary charge separation

It is interesting to compare the primary charge separation in our samples with that reported for open WT RCs, *i.e.*, with a neutral Q_A. There has been a long-standing discussion on the nature of this reaction. It is commonly accepted that this reaction is biphasic with the primary step leading to electron transfer from P* to B_A and then, from B_A^- to H_A (see Equation (1)). According to this equation, B_A^- decays faster than it is formed and this is the reason why it is so difficult to detect it in open WT RCs. However, in closed RCs, it is possible to form the state B_A^- with a higher efficiency (Figure 2). This is further confirmed by the target modelling showing that unlike in open RCs, the depopulation of the state "$P^+B_A^-$" (τ_3) is slower than its population (τ_2) for all the samples. For all samples but the AMW RC, this effect could be related to an electrostatic interaction between electrons on Q_A^- and on $(B_AH_A)^-$. However, the existence of this effect also for the AMW RC makes the previous assignement uncertain. Therefore, for the WT and AMW RCs, we also tried to exchange the τ_3 and τ_2 values in our target analysis, while leaving all the remaining intrinsic lifetimes relatively unchanged. This was done in order to make sure that τ_3 is indeed larger than τ_2. Such an exchange resulted in DADS (Figure S5C&D) of equally good quality and similar apparent lifetimes as those obtained for original fits (Figure 2A&B). However, the resulting amplitudes of the "$P^+B_A^-$" SADS were meaningless (Figure S5A&B).

Conclusions

We have shown that combination of two single point mutations, one of which accelerates charge recombination and the other decelerates it, leads to significant cancellation of the single mutations effects. Additionally, we propose a new view of both the primary charge separation and charge recombination in closed bacterial photosynthetic RCs. They may be summarized in the following way:

$$\text{Charge separation: } P^*(B_AH_A) \rightarrow P^+(B_AH_A)^-,$$

$$\text{Charge recombination: } P^+(B_AH_A)^- \rightarrow P(B_AH_A).$$

In this model, following charge separation, a fifty-fifty B_A/H_A electron delocalization ratio gradually shifts towards a higher localization of the electron on H_A due to protein dynamics. This shift is accompanied by a slowing of charge recombination. The question remains regarding what is the cause and what is an effect: whether the charge separated state induces a passive dielectric response of the protein[69] or the protein dynamics, triggered by excitation, forces the delocalization shift.[42] A mixture of both these mechanisms is also possible. Irrespective, engagement of the protein shapes the energetics and kinetics of the primary charge separation and charge recombination.

Supporting Information

Comparison of 6- and 7-exponential global fits for the ELL sample; estimation of the relative contribution of the states $P^+B_A^-$ and $P^+H_A^-$ within the compartment "$(P^+H_A^-)_1$"; Figures S1-S5.

Acknowledgements

The studies were financially supported from the project no. 2017/25/N/NZ1/02382 by KD funded by The National Science Centre (NCN).

References

(1) Blankenship, R. E.; Madigan, M. T.; Bauer, C. E. editors. *Anoxygenic photosynthetic bacteria*, Kluwer Academic Publishers, Dordrecht/Boston/London, 1995.

(2) Hunter, C. N.; Daldal, F.; Thurnauer, M. C.; Beatty, J. T. editors. *The purple phototrophic bacteria*, Springer, Dordrecht, 2009.

(3) Wydrzynski, T.J.; Satoh, K. editors. *Photosystem II: the light-driven water: plastoquinone oxidoreductase*, Springer, Dordrecht, 2005.

(4) Golbeck, J.; van der Est, A. editors. *Photosynthetic Reaction Centers in The Biophysics of Photosynthesis*, Springer, New York/Heidelberg/Dordrecht/London, 2014.

(5) Martin, J. L.; Breton, J.; Hoff, A.J.; Migus, A.; Antonetti, A. Femtosecond spectroscopy of electron transfer in the reaction center of the photosynthetic bacterium Rhodopseudomonas sphaeroides R-26: Direct electron transfer from the dimeric bacteriochlorophyll primary donor to the bacteriopheophytin acceptor with a time constant of 2.8 +/- 0.2 psec. *Proc. Natl. Acad. Sci. U S A.* **1986**, *83 (4)*, 957-961.

(6) Parson, W. W.; Warshel, A. Mechanism of Charge Separation in Purple Bacterial Reaction Centers. In: Hunter, C. N.; Daldal, F.; Thurnauer, M. C.; Beatty, J. T. *The Purple Phototrophic Bacteria*, Springer, Netherlands, 2009.

(7) Savikhin, S.; Jankowiak, R. Mechanism of Primary Charge Separation in Photosynthetic Reaction Centers. In: Golbeck, J.; van der Est, A. editors. *The Biophysics of Photosynthesis. Biophysics for the Life Sciences*, vol 11, Springer, New York, 2014.

(8) Allen, J. P.; Feher, G.; Yeates, T.O.; Komiya, H.; Rees, D. C. Structure of the reaction center from Rhodobacter sphaeroides R-26: the cofactors. *Proc. Natl. Acad. Sci. U S A.* **1987**, *84 (16)*, 5730–5734.

(9) Woodbury, N. W. T.; Allen, J. P. Electron transfer in purple nonsulfur bacteria, In: Blankenship, R. E.; Madigan, M. T.; Bauer, C. E. editors. *Anoxygenic Photosynthetic Bacteria.* Kluwer Academic Publishers: Dordrecht/Boston/London, 1995; p 527.

(10) Marchi, M.; Gehlen, J. N.; Chandler, D.; Newton, M. Diabatic surfaces and the pathway for primary electron transfer in a photosynthetic reaction center. *J. Am. Chem. Soc.* **1993**, *115*, 4178 –4190.

(11) Arlt, T.; Schmidt, S.; Kaiser, W.; Lauterwasser, C.; Meyer, M.; Scheer, H.; Zinth, W. The accessory bacteriochlorophyll: a real electron carrier in primary photosynthesis. *Proc. Natl. Acad. Sci. U.S.A.* **1993,** *90 (24)*, 11757-11761.

(12) Zinth, W.; Wachtveitl, J. The First Picoseconds in Bacterial Photosynthesis—Ultrafast Electron Transfer for the Efficient Conversion of Light Energy ChemPhysChem. **2005**, *6*, 871–880.

(13) Holzwarth, A. R.; Müller, M. G. Energetics and kinetics of radical pairs in reaction centers from Rhodobacter sphaeroides. A femtosecond transient absorption study. *Biochem.* **1996**, *35 (36)*, 11820-11831.

(14) van Stokkum, I. H.; Beekman, L. M.; Jones, M. R.; van Brederode, M. E.; van Grondelle, R. Primary electron transfer kinetics in membrane-bound Rhodobacter sphaeroides reaction centers: a global and target analysis. *Biochem.* **1997**, *36 (38)*, 11360-11368.

(15) Kaufmann, K. J.; Dutton, P. L.; Netzel, T. L.; Leigh, J. S.; Rentzepis, P. M. Picosecond kinetics of events leading to reaction center bacteriochlorophyll oxidation. *Science*. **1975**, *188 (4195)*, 1301-1304.

(16) Rockley, M. G.; Windsor, M. W.; Cogdell, R. J.; Parson, W. W. Picosecond detection of an intermediate in the photochemical reaction of bacterial photosynthesis. *Proc. Natl. Acad. Sci. U S A.* **1975**, *72 (6)*, 2251-2255.

(17) Holten, D.; Windsor, M. W.; Parson, W. W.; Thornber, J. P. Primary photochemical processes in isolated reaction centers of Rhodopseudomonas viridis. *Biochim. Biophys. Acta*. **1978**, *501 (1)*, 112-126.

(18) Volk, M.; Ogrodnik, A.; Michel-Beyerle, M. E. The Recombination Dynamics of the Radical Pair $P^{+}H^{-}$ in External Magnetic and Electric Fields. *In*: Blankenship, R. E.; Madigan, M. T.; Bauer, C. E. *Anoxygenic Photosynthetic Bacteria*; Kluwer Academic Publishers: Dordrecht, Boston, London, The Netherlands, 1995.

(19) Shuvalov, V. A.; Klimov, V. V. The primary photoreactions in the complex cytochrome-P-890 . P-760 (bacteriopheophytin 760) of Chromatium minutissimum at low redox potentials. *Biochim. Biophys. Acta.* **1967**, *440*, 587–599.

(20) Schenck, C. C.; Blankenship, R. E.; Parson, W. W. Radical-pair decay kinetics, triplet yields, and delayed fluorescence from bacterial reaction centers. *Biochim. Biophys. Acta.* **1982**, *680*, 44–59.

(21) Woodbury, N. W. T.; Parson, W. W. Nanosecond fluorescence from islolated photosynthetic reaction centers of Rhodopseudomonas sphaeroides. *Biochim. Biophys. Acta.* **1984**, *767 (2)*, 345-361.

(22) Woodbury, N. W.; Parson, W. W.; Gunner, M. R.; Prince, R. C.; Dutton, P. L. Radical-pair energetics and decay mechanisms in reaction centers containing

anthraquinones, naphthoquinones or benzoquinones in place of ubiquinone. *Biochim. Biophys. Acta.* **1986**, *851*, 6–22.

(23) Ogrodnik, A.; Keupp, W.; Volk, M.; Aumeier, G.; Michel-Beyerle, M. E. J. Inhomogeneity of Radical Pair Energies in Photosynthetic Reaction Centers Revealed by Differences in Recombination Dynamics of P+HA- When Detected in Delayed Emission and in Absorption. *J. Phys. Chem.* **1994**, *98 (13)*, 3432–3439.

(24) Hartwich, G.; Lossau, H.; Michel-Beyerle, M. E.; Ogrodnik, A. Nonexponential Fluorescence Decay in Reaction Centers of Rhodobacter sphaeroides Reflecting Dispersive Charge Separation up to 1 ns. *J. Phys. Chem. B.* **1998**, *102*, 3815-3820.

(25) Tang, C. K.; Williams, J. C.; Taguchi, A. K. W.; Allen, J. P.; Woodbury, N. W. P+HA- Charge Recombination Reaction Rate Constant in Rhodobacter sphaeroides Reaction Centers is Independent of the P/P+ Midpoint Potential. *Biochem.* **1999**, 38, 8794-8799.

(26) Shuvalov, V. A.; Parson, W. W. Energies and kinetics of radical pairs involving bacteriochlorophyll and bacteriopheophytin in bacterial reaction centers. *Proc. Natl. Acad. Sci. U.S.A.* **1981**, *78*, 957-961.

(27) Ridge, J.P.; van Brederode, M.E.; Goodwin, M.G.; van Grondelle, R.; Jones M. R. Mutations that modify or exclude binding of the QA ubiquinone and carotenoid in the reaction center from Rhodobacter sphaeroides. *Photosynth. Res.* **1999**, *59***,** 9–26.

(28) McAuley, K.E.; Fyfe, P.K.; Ridge, J. P.; Cogdell, R. J.; Isaacs, N.W.; Jones M. R.; Ubiquinone binding, ubiquinone exclusion, and detailed cofactor conformation in a mutant bacterial reaction center. *Biochem.* **2000**, *39 (49)*, 15032-15043.

(29)Woodbury, N. W.; Becker, M.; Middendorf, D.; Parson, W. W. Picosecond kinetics of the initial photochemical electron-transfer reaction in bacterial photosynthetic reaction centers. *Biochem.* **1985**, *24 (26)*, 7516–7521.

(30) Wang, S.; Lin, S.; Lin, X.; Woodbury, N. W.; Allen, J. P. Comparative study of reaction centers from purple photosynthetic bacteria: Isolation and optical spectroscopy. *Photosynth. Res*. **1994,** *42 (3)*, 203-215.

(31) Gibasiewicz, K.; Pajzderska, M. Primary Radical Pair P+H - Lifetime in Rhodobacter sphaeroides with Blocked Electron Transfer to QA. Effect of o-Phenanthroline. *J. Phys. Chem. B.* **2008**, *112 (6)*, 1858-1865.

(32) Gibasiewicz, K.; Pajzderska, M.; Ziółek, M.; Karolczak, J.; Dobek, A. Internal Electrostatic Control of the Primary Charge Separation and Recombination in Reaction Centers from Rhodobacter sphaeroides Revealed by Femtosecond Transient Absorption. *J. Phys. Chem. B.* **2009**, *113 (31)*, 11023-11031.

(33) Gibasiewicz, K.; Pajzderska, M.; Potter, J. A.; Fyfe, P. K.; Dobek, A.; Brettel, K.; Jones, M. R. Mechanism of Recombination of the P+HA - Radical Pair in Mutant Rhodobacter sphaeroides Reaction Centers with Modified Free Energy Gaps Between P +BA - and P+HA - . *J. Phys. Chem. B.* **2011**, *115 (44)*, 13037-13050.

(34) Gibasiewicz, K.; Pajzderska, M.; Dobek, A.; Karolczak, J.; Burdziński, G.; Brettel, K.; Jones, M. R. Analysis of the Temperature-Dependence of P+HA - Charge Recombination in the Rhodobacter sphaeroides Reaction Center Suggests Nanosecond Temperature-Independent Protein Relaxation. *Phys. Chem. Chem. Phys*. **2013**, *15*, 16321-16333.

(35)Wang, H.; Hao, Y.; Jiang, Y.; Lin, S.; Woodbury, N. W. Role of protein dynamics in guiding electron-transfer pathways in reaction centers from Rhodobacter sphaeroides. *J Phys Chem B.* **2012,** *116 (1)*, 711-717.

(36) Frauenfelder, H. *The Physics of Proteins: An Introduction to Biological Physics and Molecular Biophysics;* Springer-Verlag: New York, 2011.

(37) Warshel, A.; Chu, Z. T.; Parscon, W. W.; Dispersed polaron simulations of electron transfer in photosynthetic reaction centers. *Science*. **1989,** *246*, 112-116.

(38) Gehlen, J. N.; Marchi, M.; Chandler, D.; Dynamics affecting the primary charge transfer in photosynthesis. *Science* **1994**, *263*, 499-502.

(39) Graige, M. S.; Feher, G.; Okamura, M. Y. Conformational gating of the electron transfer reaction QA-QB/QAQB-. in bacterial reaction centers of Rhodobacter sphaeroides determined by a driving force assay. *Proc. Natl. Acad. Sci. U.S.A.* **1998**, *95*, 11679–11684.

(40) McMahon, B. H.; Muller, J. D.; Nienhaus, G. U. Electron transfer and protein dynamics in the photosynthetic reaction center. *Biophys. J.* **1998**, *74*, 2567–2587.

(41) Parson, W. W.; Warshel, A. Dependence of Photosynthetic Electron-Transfer Kinetics on Temperature and Energy in a Density-Matrix Model
J. Phys. Chem. B. **2004,** *108*, 10474-10483.

(42)Wang, H.; Lin, S.; Allen, J. P.; Williams, J. A. C.; Blankert, S.; Laser, C.; Woodbury, N. W. Protein dynamics control the kinetics of initial electron transfer in photosynthesis. *Science.* **2007**, *316 (5825)*, 747-750.

(43) Pawlowicz, N. P.; van Grondelle, R.; van Stokkum, I. H. M.; Jones, M. R.; Breton, J.; Groot, M. L. Identification of the first steps in charge separation in bacterial photosynthetic reaction centers of Rhodobacter sphaeroides by ultrafast mid-infrared

spectroscopy: Electron transfer and protein dynamics. *Biophys. J.* **2008**, *95*, 1268–1284.

(44) Guo, Z.; Woodbury, N. W.; Pan, J.; Lin, S. Protein Dielectric Environment Modulates the Electron-Transfer Pathway in Photosynthetic Reaction Centers. *Biophys. J.* **2012**, *103*, 1979–1988.

(45) LeBard, D. N.; Matyushov, D. V. Energetics of Bacterial Photosynthesis. *J. Phys. Chem. B.* **2009**, *113*, 12424–12437.

(46) LeBard, D. N.; Matyushov, N. D. Protein–water electrostatics and principles of bioenergetics. *Phys. Chem. Chem. Phys.* **2010**, *12*, 15335–15348.

(47) LeBard, D. N.; Martin, D. R.; Lin, S.; Woodbury N. W.; Matyushov, D. V. Protein dynamics to optimize and control bacterial photosynthesis. *Chem. Sci.* **2013**, *4*, 4127-–4136.

(48) Gibasiewicz, K.; Białek, R.; Pajzderska, M.; Karolczak, J.; Burdziński, G.; Jones, M. R.; Brettel, K. Weak temperature dependence of P (+) H A (-) recombination in mutant Rhodobacter sphaeroides reaction centers. *Photosynth Res.* **2016**, *128 (3)*, 243-258.

(49) McAuley-Hecht, K. E.; Fyfe, P. K.; Ridge, J. P.; Prince, S. M.; Hunter, C. N.; Isaacs, N. W.; Cogdell, R. J.; Jones, M. R. Structural studies of wild-type and mutant reaction centers from an antenna-deficient strain of Rhodobacter sphaeroides: monitoring the optical properties of the complex from bacterial cell to crystal. *Biochem.* **1998**, *37*, 4740–4750.

(50) Jones, M. R.; Fowler, G. J. S.; Gibson, L. C. D.; Grief, G. G.; Olsen, J. D.; Crielaard, W.; Hunter, C. N. Mutants of Rhodobacter sphaeroides lacking one or more pigment-protein complexes and complementation with reaction-centre, LH1, and LH2 genes. *Mol. Microbiol.* **1992**, *6*, 1173–1184.

(51) Jones, M. R.; Heer-Dawson M.; Mattioli T. A.; Hunter, C. N.; Robert, B.; Site-specific mutagenesis of the reaction centre from Rhodobacter sphaeroides studied by Fourier transform Raman spectroscopy: mutations at tyrosine M210 do not affect the electronic structure of the primary donor. *FEBS Lett.* **1994**, *339 (1-2)*, 18-24.

(52) Bylina, E. J.; Kirmaier, C.; McDowell, L.; Holten, D.; Youvan,D. C. Influence of an amino-acid residue on the optical properties and electron transfer dynamics of a photosynthetic reaction centre complex. *Nature* **1988**, *336*, 182–184.

(53)Lin, X.; Murchison, H. A.; Nagarajan, V.; Parson, W. W.; Allen, J. P.; Williams, J. C. Specific alteration of the oxidation potential of the electron donor in reaction centers from Rhodobacter spaeroides. *Proc. Natl. Acad. Sci. U.S.A.* **1994**, *91*, 10265–10269.

(54) Wendel M, Nizinski S, Tuwalska D, Starzak K, Szot D, Prukala D, Sikorski M, Wybraniec S, Burdzinski G. Time-resolved spectroscopy of the singlet excited state of betanin in aqueous and alcoholic solutions. *Phys. Chem. Chem. Phys.* **2015**, *17 (27)*, 18152-18158.

(55) Snellenburg, J. J.; Laptenok, S.; Seger, R.; Mullen, K. M.; van Stokkum, I. H. M. Glotaran: a java-based graphical user interface for the R package TIMP. *J. Stat. Softw.* **2012**, *49 (3)*, 1–22.

(56) Jia, Y.; Jonas, D. M.; Nagasawa, T. J. Y.; Lang, M. J.; Fleming, G. R. Observation of Ultrafast Energy Transfer from the Accessory Bacteriochlorophylls to the Special Pair in Photosynthetic Reaction Centers. *J. Phys. Chem* **1995**, *99*, 6263-6266.

(57) Jonas, D. M.; Lang, M. J.; Nagasawa, Y.; Joo, T.; Fleming, G. R. Pump−Probe Polarization Anisotropy Study of Femtosecond Energy Transfer within the Photosynthetic Reaction Center of Rhodobacter sphaeroides R26. *J. Phys. Chem.* **1996**, *100*, 12660-12673.

(58) Stanley, R. J.; King, B.; Boxer, G. Excited State Energy Transfer Pathways in Photosynthetic Reaction Centers. 1. Structural Symmetry Effects. *J. Phys. Chem.* **1996**, *100*, *29*, 12052-12059**.**

(59) King, B. A.; McAnaney, T.; deWinter, A.; Boxer S. G. Excited State Energy Transfer Pathways in Photosynthetic Reaction Centers. 3. Ultrafast Emission from the Monomeric Bacteriochlorophylls *J. Phys. Chem. B.* **2000**, *104*, 8895-8902.

(60) Jordanides, X. J.; Scholes, G. D.; Fleming, G. R. The Mechanism of Energy Transfer in the Bacterial Photosynthetic Reaction Center. *J. Phys. Chem. B.* **2001**, *105*, 1652-1669.

(61) van Brederode, M. E.; Jones, M. R.; van Mourik, F.; van Stokkum, I. H. M.; van Grondelle, R. A new pathway for transmembrane electron transfer in photosynthetic reaction centers of Rhodobacter sphaeroides not involving the excited special pair. *Biochem.* **1997**, *36*, 6855–6861.

(62) van Brederode, M. E.; van Mourik, F.; van Stokkum, I. H. M.; Jones, M.R.; van Grondelle, R. Multiple pathways for ultrafast transduction of light energy in the photosynthetic reaction center of Rhodobacter sphaeroides. *Proc. Natl. Acad. Sci. U.S.A.* **1999**, *96*, 2054–2059.

(63) Fajer, J.; Brune, D. C.; Davis, M. S.; Forman, M.; Spaulding, L. D. Primary charge separation in bacterial photosynthesis: Oxidized chlorophylls and reduced pheophytin. *Proc. Natl. Acad. Sci. U.S.A.* **1975**, *72 (12)*, 4956-4960.

(64) Peloquin, J. M.; Williams, A. C.; Lin, X.; Alden, R. G.; Taguchi, A. K. W.; Allen, J. P.; Woodbury, N. W. Relationship between thermodynamics and mechanism during photoinduced charge separation in reaction centers from Rhodobacter sphaeroides. *Biochem.* **1994**, *33*, 8089-8100.

(65) Lin, S.; Taguchi, A. K. W.; Woodbury, N. W. Excitation Wavelength Dependence of Energy Transfer and Charge Separation in Reaction Centers from Rhodobacter sphaeroides: Evidence for Adiabatic Electron Transfer. *J. Phys. Chem.* **1996**, *100*, 17067-17078.

(66) Zhu, J.; van Stokkum, I. H. M.; Paparelli, L.; Jones, M. R.; Groot, M. L. Early Bacteriopheophytin Reduction in Charge Separation in Reaction Centers of *Rhodobacter sphaeroides*. *Biophys. J.* **2013**, *104*, 2493–2502.

(67) Heller, B. A.; Holten, D.; Kirmaier, C. Effects of Asp residues near the L-side pigments in bacterial reaction centers. *Biochem.* **1996**, *35*, 15418-15427.

(68) Katilius, E.; Turanchik, T.; Lin, S.; Taguchi, A. K. W.; Woodbury, N. W. B-Side Electron Transfer in a Rhodobacter sphaeroides Reaction Center Mutant in Which the B-Side Monomer Bacteriochlorophyll Is Replaced with Bacteriopheophytin. *J. Phys. Chem. B.* **1999**, *103*, 7386-7389.

(69) Dubas, K.; Baranowski, M.; Podhorodecki, A.; Jones, M. R.; Gibasiewicz, K. Unified Model of Nanosecond Charge Recombination in Closed Reaction Centers from Rhodobacter sphaeroides: Role of Protein Polarization Dynamics. *J. Phys. Chem. B.* **2016**, *120*, 4890−4896.

Tables

Table 1. Comparison of the parameters of the equilibria "$P^+B_A^-$"↔"$(P^+H_A^-)_1$"[a] and $P^+B_A^-$ ↔$P^+H_A^-$ (within the compartment "$(P^+H_A^-)_1$") for the samples under study.

RC	["$(P^+H_A^-)_1$"]/["$P^+B_A^-$"] = τ_8/τ_3[b]	["$P^+B_A^-$"]$_{rel}$[c]	["$P^+H_A^-$"]$_{rel}$[c]	ΔG[d] [mV]	$[P^+B_A^-]_{rel}$[e]	$[P^+H_A^-]_{rel}$[e]	ΔG_1[f] [mV]
WT	63	1.6%	98.4%	104	2.8%	97.8%	88
AMW	-	-	-	-	5%	95%	74
ELL	2.4	29%	71%	22	30%	70%	21
ELL/AMW	7.3	12%	88%	50	14%	86%	45

[a] "$P^+B_A^-$" and "$(P^+H_A^-)_1$" denote initial and secondary charge separated states, respectively, both composed of unresolved virtual pure states $P^+B_A^-$ and $P^+H_A^-$.

[b] Parameters ["$P^+B_A^-$"] and ["$(P^+H_A^-)_1$"] are the equilibrium concentrations of the respective states included in the target analysis in Figure 5; τ_3 and τ_8 are lifetimes defined in scheme A in Figure 5.

[c] Parameters ["$P^+B_A^-$"]$_{rel}$ and ["$P^+H_A^-$"]$_{rel}$ are the relative populations of the states "$P^+B_A^-$" and "$(P^+H_A^-)_1$" that are in equilibrium with one another.

[d] ΔG is the absolute value of the free energy gap between the states "$(P^+H_A^-)_1$" and "$P^+B_A^-$", estimated from Eq. 3.

[e] Parameters $[P^+B_A^-]_{rel}$ and $[P^+H_A^-]_{rel}$ are the relative populations of the states $P^+B_A^-$ and $P^+H_A^-$ that are in the equilibrium with one another within the state "$(P^+H_A^-)_1$" (or $P^+(B_AH_A)_1^-$).

[f] ΔG_1 is the absolute value of the free energy gap between the states $P^+B_A^-$ and $P^+H_A^-$ that contribute to the state "$(P^+H_A^-)_1$", estimated from Eq. S5.

Figures

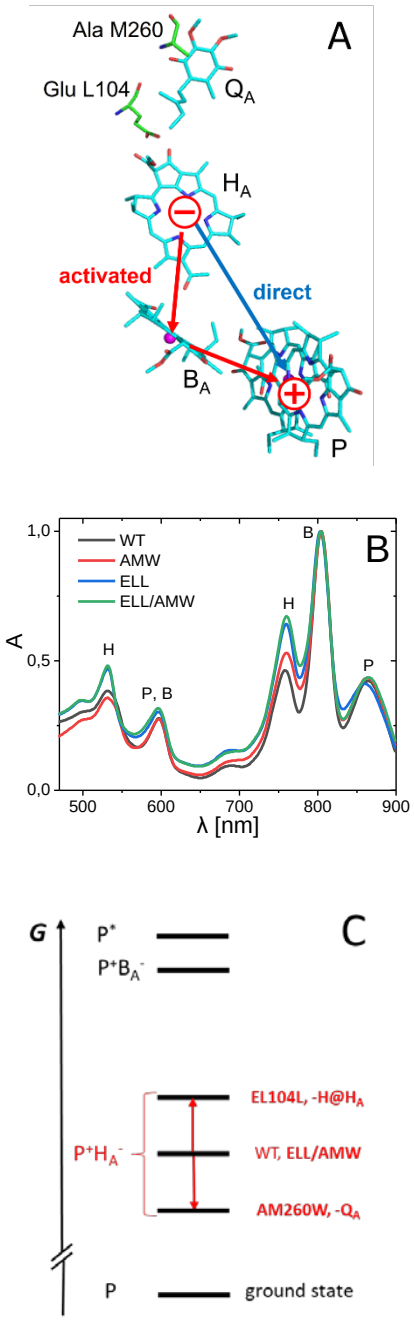

Figure 1. (A) Arrangement of the electron transfer cofactors in the wild type *Rhodobacter sphaeroides* RC. Amino acids replaced in the mutant strains as well as postulated direct and activated back ET routes are also shown. (B) Ground-state absorption spectrum of the WT and mutant RCs normalized at ~804 nm. (C) Comparison of the expected effects of the single (ELL, AMW) and double (ELL/AMW) point mutations on the relative free energy level of the state $P^+H_A^-$.

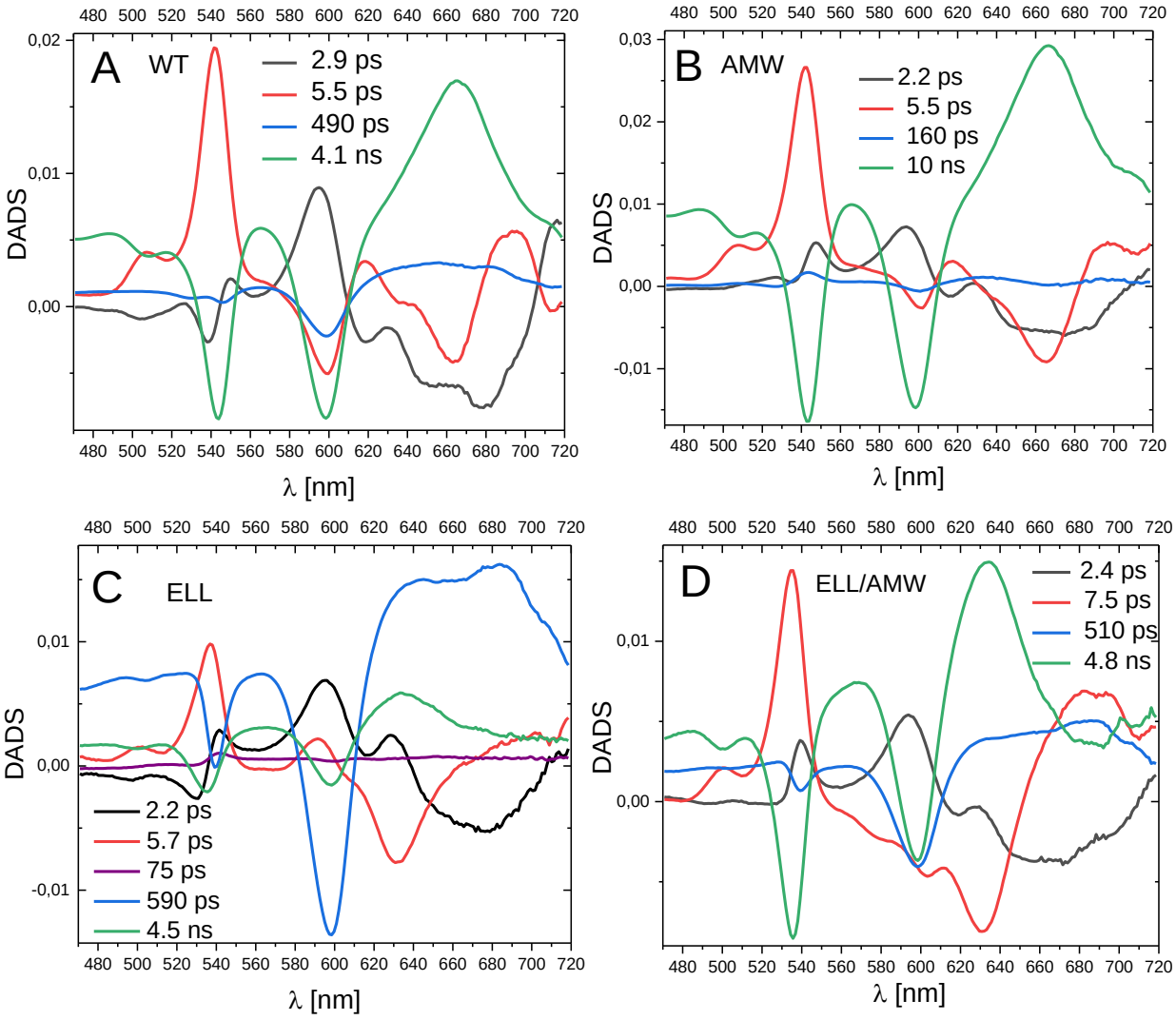

Figure 2. Decay associated difference spectra for the WT and mutant RCs.

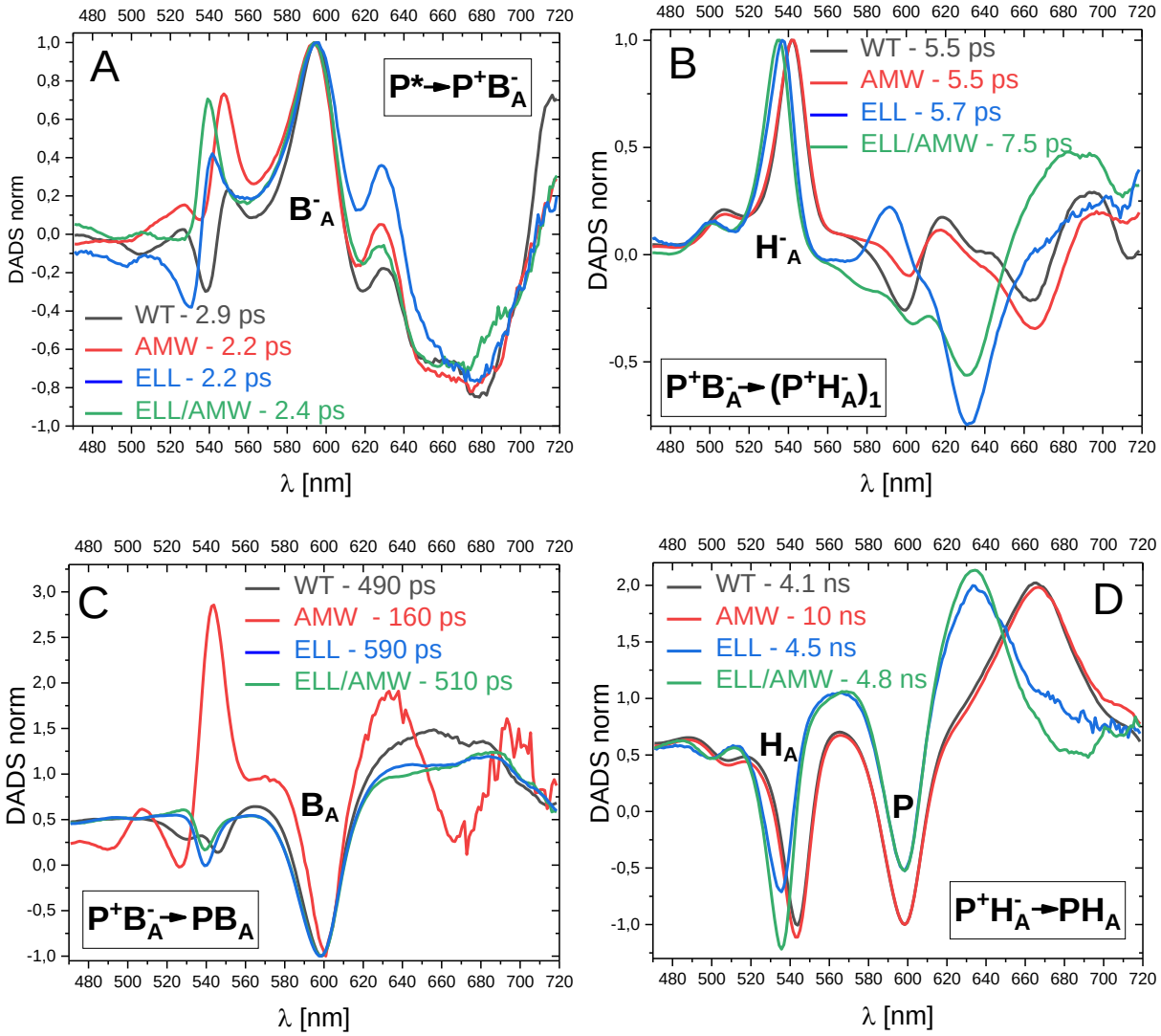

Figure 3. Comparison of the lineshapes of normalized DADS obtained for the four RCs. (A) – ~2.5-ps DADS normalized at ~595 nm; (B) – ~6-ps DADS normalized at ~540 nm; (C) – hundreds-ps DADS normalized at ~600 nm; (D) – nanosecond DADS normalized in such a way that the depth of the P photobleaching band at 598 nm relative to the signal at 565 nm was the same for all spectra. (A-D) – the labels in the black rectangles indicate the reactions dominating the respective kinetic phases.

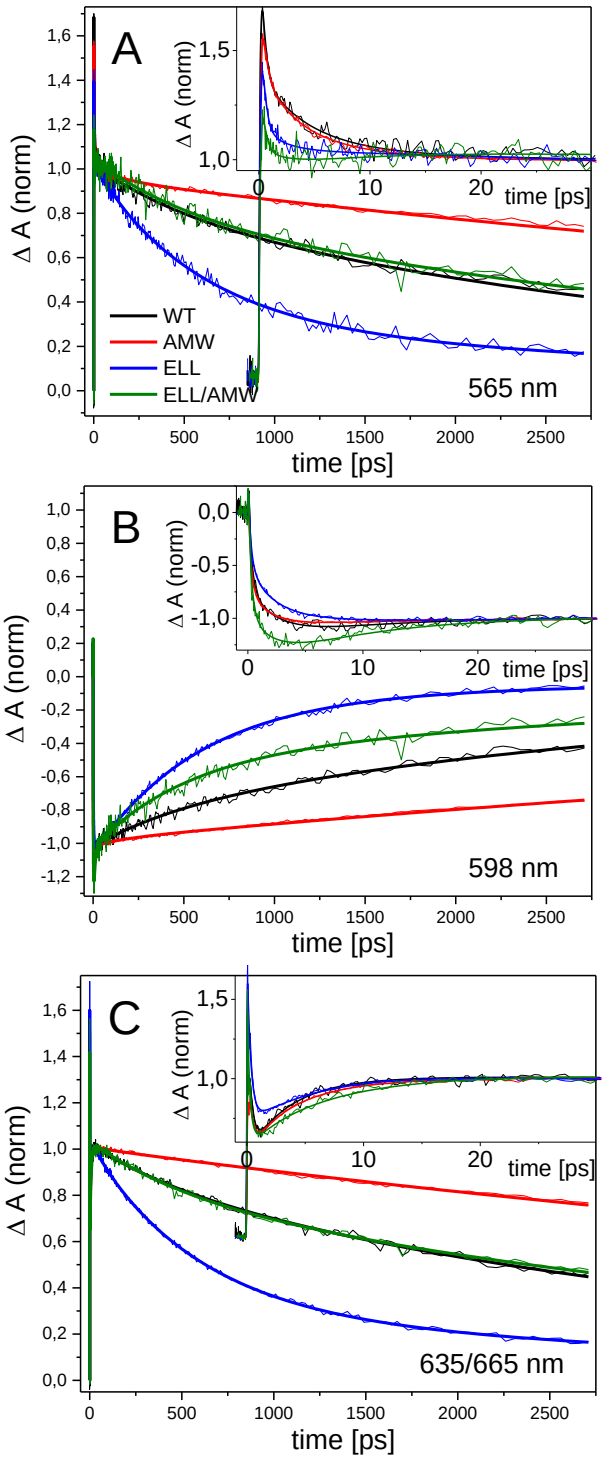

Figure 4. Comparisons of the ET kinetics at three selected wavelengths in the four RCs, normalized at ~30 ps after excitation: (A) – 565 nm; (B) – 598 nm; (C) – 635 nm (ELL, ELL/AMW)/665 nm (WT, AMW). Insets: respective kinetics in 30-ps time windows. Fits are from the global analysis presented in Figure 2.

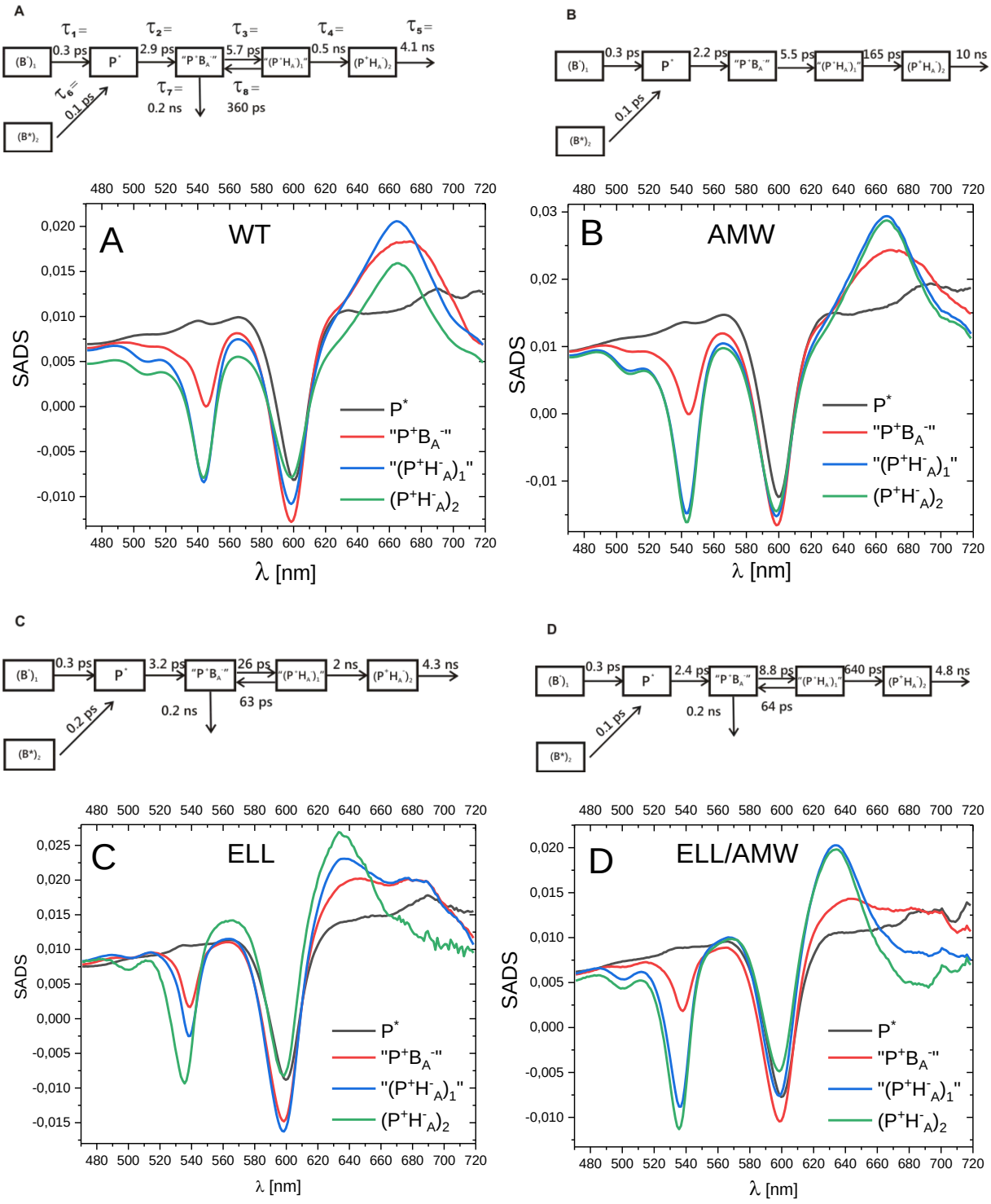

Figure 5. Species associated difference spectra of the WT and three mutant RCs.

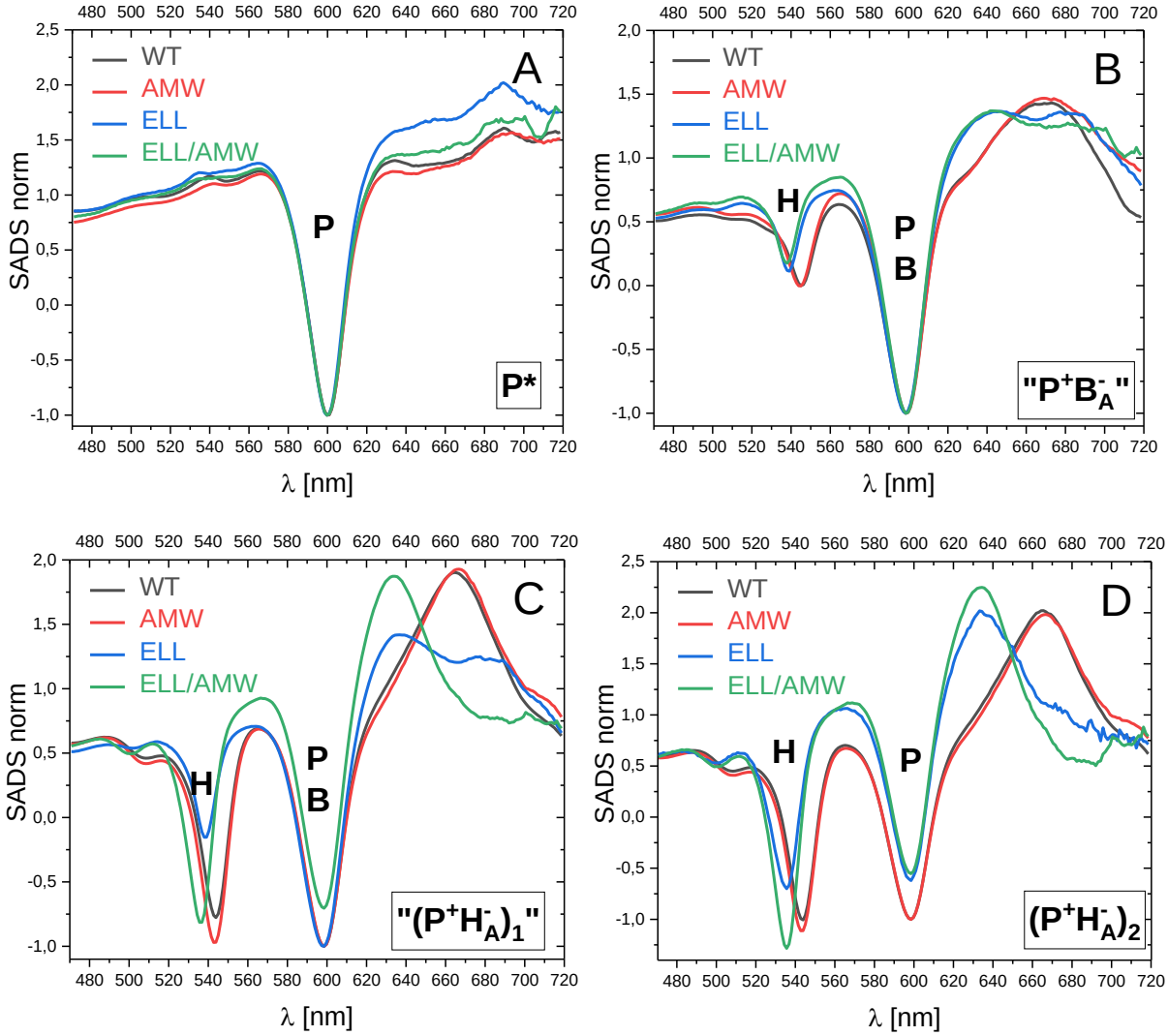

Figure 6. Comparisons of the line shapes of analogous SADS for the four RCs. (A, B) – spectra of the compartments P* and "$P^+B_A^-$", respectively, normalized at ~600 nm; (C, D) – spectra of the compartments "$(P^+H_A^-)_1$" and $(P^+H_A^-)_2$ normalized in such a way that the depth of the ~600-nm photobleaching band relative to the amplitude at 565 nm is the same for all the samples.

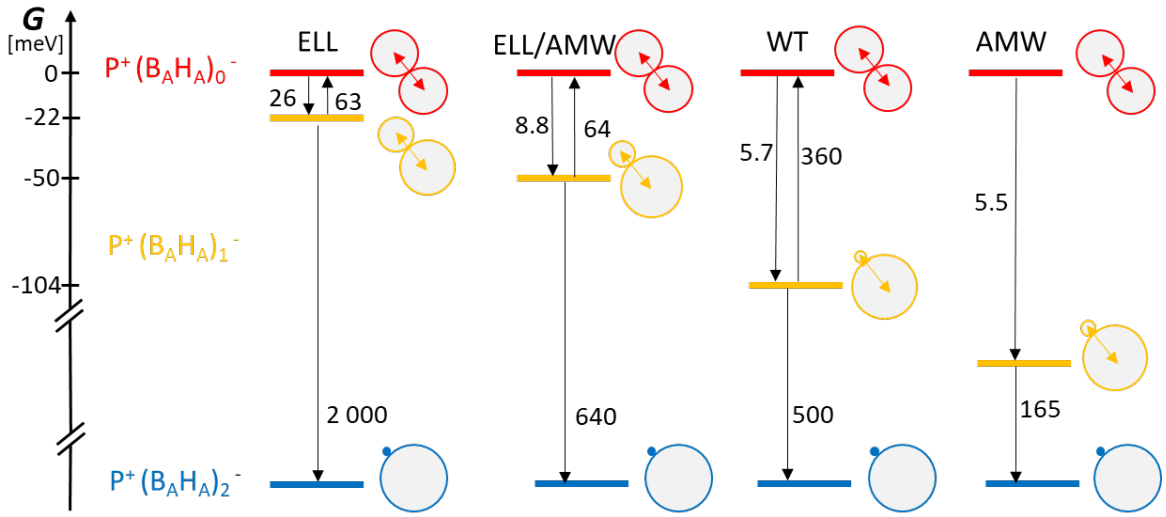

Figure 7. Energetic model of relaxation of the charge separated state $P^+(B_AH_A)^-$ for the four RCs. The initially formed charge separated state is in red, the intermediate state is in yellow, and the final resolved charge separated state is in blue. The circles represent B_A (upper-left circle in each pair) and H_A (lower-right circle in each pair), and their areas are proportional to the probability of localization of the electron on B_A or H_A. The numerical values for these probabilities are given in Table 1 (columns $[P^+B_A^-]_{rel}$ and $[P^+H_A^-]_{rel}$). The numbers in black at the arrows are the molecular lifetimes (in picoseconds) obtained from the target analysis (see Figure 5). Note that the free energy level of the state $P^+(B_AH_A)_0^-$ was arbitrarily set at 0 meV, while the free energy level of the state $P^+(B_AH_A)_2^-$ (and $P^+(B_AH_A)_1^-$ for AMW) was not determined.

TOC Graphic

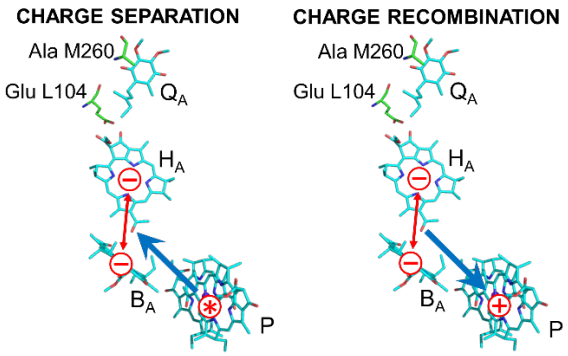
CHARGE SEPARATION
Ala M260
Glu L104
Q_A
H_A
B_A
P
CHARGE RECOMBINATION
Ala M260
Glu L104
Q_A
H_A
B_A
P

Supporting Information

Antagonistic Effects of Point Mutations on Charge Recombination and a New View of Primary Charge Separation in Photosynthetic Proteins

K. Dubas,[1, 3] , S. Szewczyk,[1] Rafał Białek [1], G. Burdziński,[1] M. R. Jones,[2] K. Gibasiewicz[1]*

[1] Faculty of Physics, Adam Mickiewicz University, ul. Uniwersytetu Poznanskiego 2, 61-614 Poznań, Poland.

[2] School of Biochemistry, Medical Sciences Building, University of Bristol, University Walk, Bristol, BS8 1TD, UK

[3] Department of Optometry, Poznan University of Medical Sciences, ul. Rokietnicka 5d, 60-806 Poznań, Poland

* Corresponding author; e-mail: krzyszgi@amu.edu.pl; tel: +48 61 8296390

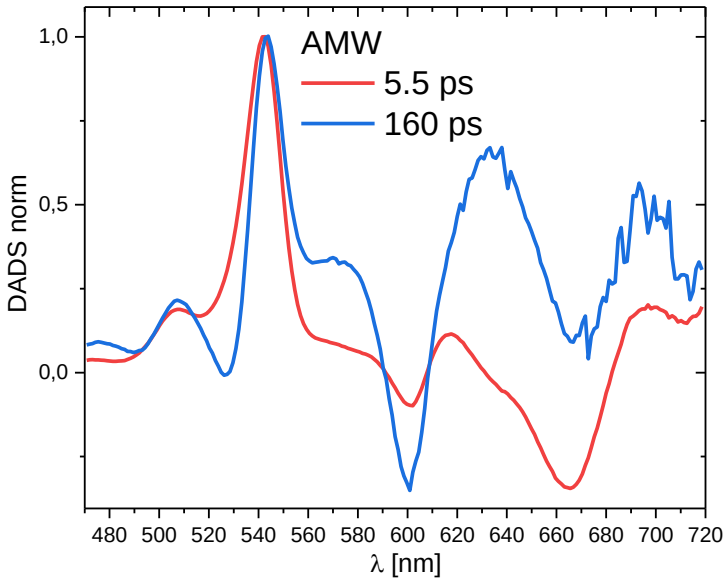

Figure S1. Comparison of the 5.5-ps and 160-ps DADS for the AMW RC normalized at ~542 nm.

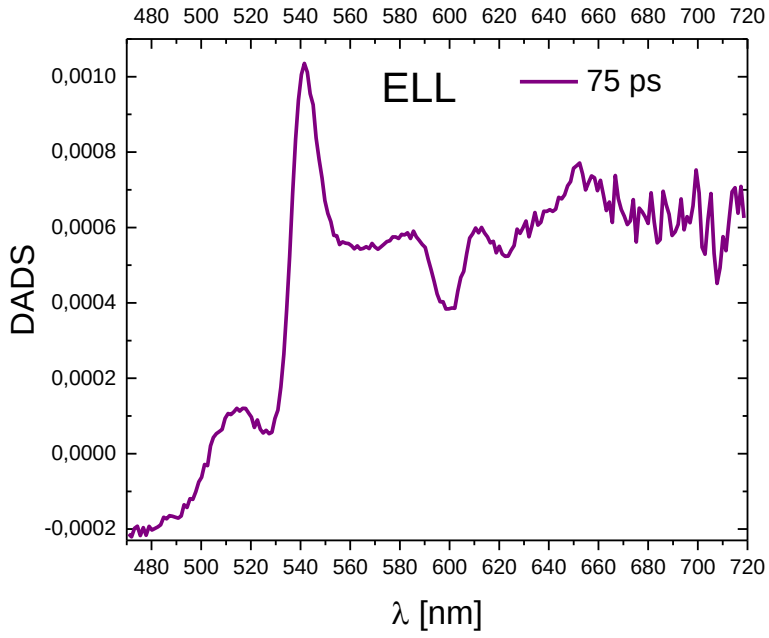

Figure S2. The 75-ps DADS of the ELL RC from Fig. 2C extended in the vertical direction.

Comparison of 6- and 7-exponential global fits for the ELL sample

The corresponding 570/590-ps DADS and 4.2/4.5-ns DADS for the ELL RC are of very similar shapes for the 6- and 7-exponential global fits (compare spectra in Figs. S3 and 2C). An extra component of ~75-ps lifetime in the 7-exponential fit caused shortening of the 3.2-ps and 17-ps components (resolved in the 6-exponential fit) to 2.2 and 5.7 ps, respectively (in the 7-exponential fit). Moreover, introduction of the ~75-ps DADS resulted in the shape and lifetime of the 2.2-ps DADS being very similar to those resolved for the three remaining RCs (Fig. 3A).

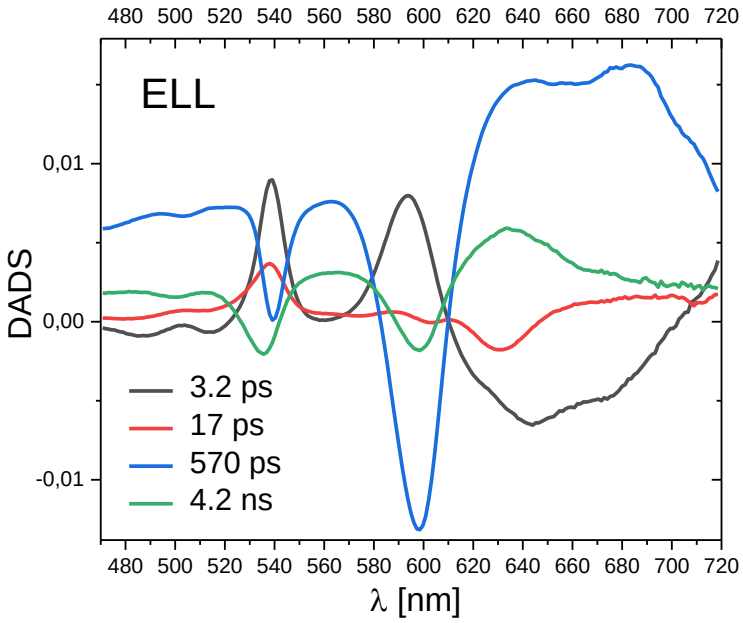

Figure S3. Decay associated difference spectra for the ELL RC resulting from the six-exponential model (the two fastest subpicosecond DADS are not shown) associated with the compartmental model shown in Fig. 5C.

Estimation of the relative contribution of the states $P^+B_A^-$ and $P^+H_A^-$ within the compartment "$(P^+H_A^-)_1$"

In the following we describe the way in which we estimated the relative contributions of the states $P^+B_A^-$ and $P^+H_A^-$ within the compartment "$(P^+H_A^-)_1$" in the ELL/AMW RC. Estimations for the remaining RCs were made in an analogous way.

We assumed that the $(P^+H_A^-)_2$ SADS in Fig. S4 represents pure $P^+H_A^-$ state. Consequently, we assumed that the negative band of this SADS at ~540 nm is exclusively due to photobleaching of the H_A Q_x band whereas the negative band at ~600 nm is exclusively due to photobleaching of the P Q_x band. From the relative amplitudes of these bands, ΔA_H and ΔA_P, using the Lambert-Beer law, we estimated the ratio of differential molar extinction coefficients of these two molecules at the respective wavelengths:

$$\Delta\varepsilon_{H,540}/\Delta\varepsilon_{P,600} = \Delta A_H/\Delta A_P = 1.17. \quad \text{(S1)}$$

The method for determining the amplitudes ΔA_H and ΔA_P shown in Fig. S4 is somewhat arbitrary but we cannot see any clear advantage of different methods to estimate these quantities.

Next we assumed that the "$(P^+H_A^-)_1$" SADS in Fig. S4 represents a mixture of the states $P^+H_A^-$ and $P^+B_A^-$, and that the differential molar extinction coefficient of B_A at ~600 nm, $\Delta\varepsilon_{B,600}$, is the same as that of P at ~600 nm and, for simplicity, assumed to be equal to 1 (arbitrary unit):

$$\Delta\varepsilon_{B,600} = \Delta\varepsilon_{P,600} = 1. \quad \text{(S2)}$$

We also assumed that the relaxation state of the protein does not affect the values of $\Delta\varepsilon_{H,540}$ and $\Delta\varepsilon_{P,600}$, meaning that they are the same for the compartments "$(P^+H_A^-)_1$" and $(P^+H_A^-)_2$.

Under these assumptions we could estimate the relative concentrations c_{PH} and c_{PB} (arbitrary unit) of the two states contributing to the "$(P^+H_A^-)_1$" compartment, $P^+H_A^-$ and $P^+B_A^-$, respectively, from the following set of linear equations obtained from the Lambert-Beer law:

- at ~540 nm

$$c_{PH}\,\Delta\varepsilon_{H,540} = \Delta A_H, \quad \text{(S3)}$$

- at ~600 nm

$$c_{PH}\,\Delta\varepsilon_P + c_{PB}\,(\Delta\varepsilon_B + \Delta\varepsilon_P) = \Delta A, \quad \text{(S4)}$$

where ΔA_H and ΔA are amplitudes of the ~540 and ~600-nm bands of the "$(P^+H_A^-)_1$" SADS, as shown in Fig. S4.

Finally, we estimated the free energy gap, ΔG_1, between the states $P^+H_A^-$ and $P^+B_A^-$ contributing to the compartment "$(P^+H_A^-)_1$":

$$\Delta G_1 = kT \ln (c_{PH}/c_{PB}), \quad \text{(S5)}$$

where k stands for a Boltzmann constant and T - an absolute temperature ($kT \approx 25$ meV).

In the case of WT sample, due to larger amplitude of "$(P^+H_A^-)_1$" SADS at ~540 nm than that of the $(P^+H_A^-)_2$ SADS, the latter one was multiplied by the arbitrarily selected correction factor of 1.3, the minimal value necessary to obtain consistent results.

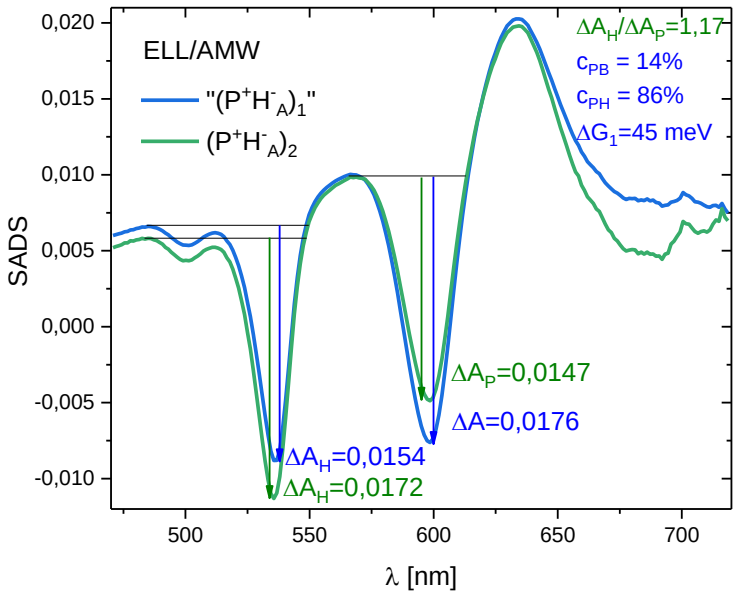

Figure S4. Graphical illustration on the determination of energetic parameters from the negative SADS bands amplitudes associated with the states "$(P^+H_A^-)_1$" and $(P^+H_A^-)_2$ of the ELL/AMW RC (spectra redrawn from Fig. 5D). ΔA_H – amplitude of the signal at ~540 nm ascribed to photobleaching of the H_A Q_x band; ΔA_P – amplitude of the signal at ~600 nm ascribed to photobleaching of the P Q_x band. See text for further details.

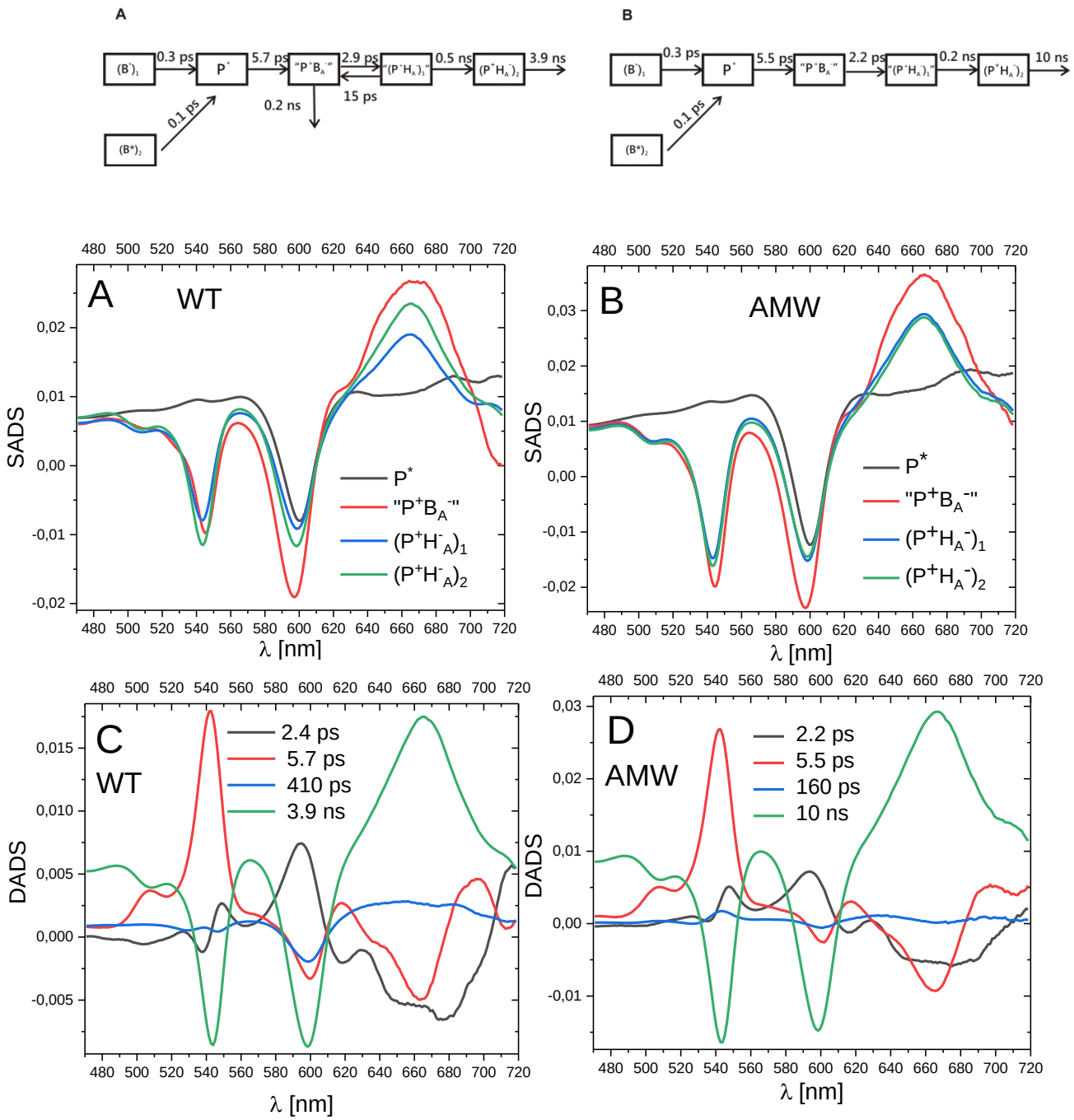
A
B
0.3 ps
5.7 ps
2.9 ps
0.5 ns
3.9 ns
0.2 ns
15 ps
0.1 ps
5.5 ps
2.2 ps
0.2 ns
10 ns
A WT
B AMW
SADS
λ [nm]
P*
"P+BA-"
(P+HA-)1
(P+HA-)2
C WT
D AMW
DADS
2.4 ps
5.7 ps
410 ps
3.9 ns
2.2 ps
5.5 ps
160 ps
10 ns

Figure S5. Results of target (A, B) and global (C, D) analysis for the WT and AMW RCs with molecular lifetime values τ_3 and τ_4 taken from Fig. 5A&B but exchanged and fixed. The remaining fit parameters were not fixed.